Title
Anatomical and functional analysis of aquaporin I in the nociceptive and olfactory sensory systems

Author
Shields, Shannon D

Publication Date
2006

Peer reviewed|Thesis/dissertation

Anatomical and functional analysis of aquaporin 1 in the nociceptive and olfactory sensory systems

by

Shannon D. Shields

DISSERTATION

Submitted in partial satisfaction of the requirements for the degree of

DOCTOR OF PHILOSOPHY

in

Neuroscience

in the

GRADUATE DIVISION

of the

UNIVERSITY OF CALIFORNIA, SAN FRANCISCO

Anatomical and functional analysis of aquaporin 1 in the nociceptive and olfactory sensory systems

Shannon D. Shields

Abstract

The water channel aquaporin 1 (AQP1) is expressed in a variety of tissues that are known to contribute to fluid balance in the body, including kidney, choroid plexus, and vascular endothelium. However, we have also discovered that AQP1 is expressed in the nervous system, in a remarkably limited distribution that includes primary afferent sensory neurons that transduce noxious stimuli and also includes the olfactory bulb. The work presented in this dissertation describes these findings in detail.

AQP1 immunoreactivity was detected in a subset of neurons of the dorsal root and trigeminal ganglia that express markers of nociceptive neurons, including substance P, IB4, and the capsaicin receptor, TRPV1. Ultrastructural studies showed that the protein is present on the plasma membrane of these neurons. AQP1 expression begins at embryonic day 15.5, similar to the time when these neurons begin to form connections within the spinal cord. The very restricted expression of AQP1 in nociceptors led us to hypothesize that it may contribute to nociceptive function. However, neither electrophysiological assessment of responsivity to noxious thermal stimulation nor behavioral testing using a comprehensive battery of assays for acute and persistent nociception illuminated differences between normal mice and mice with a null mutation for AQP1. Thus, our studies demonstrate that despite the abundant and restricted expression of AQP1 in nociceptive primary afferent

neurons, this water channel is not required for normal pain processing, and the physiological function of neuronal AQP1 for the moment remains unresolved.

In addition to primary sensory neurons, AQP1 is also present in a dense meshwork of fine fibers that cover the superficial surface of the olfactory bulb. We have found evidence that the olfactory bulb AQP1 immunoreactivity does not derive from olfactory receptor neurons, olfactory ensheathing glia, astrocytes, periglomerular cells, or trigeminal axons. Instead, we propose that AQP1 may be a marker of a unique, previously unrecognized fiber tract in the mouse olfactory bulb.

Table of Contents

Chapter 1

Introduction to aquaporins and to nociceptive processing in the peripheral nervous system and spinal cord

The aquaporins comprise an ancient family of integral membrane proteins that function as water-selective channels in animals, plants, and microorganisms. To date, thirteen mammalian aquaporins have been identified (for review, see Castle, 2005). AQP1, the archetypal member of this family, is a constitutively open, bidirectional water channel expressed in red blood cells, renal proximal tubules, capillary endothelium, choroid plexus, and other water permeable tissues (Agre et al., 2002). It is a small integral membrane protein (~28 kDa) that contains six transmembrane domains, with both the N- and C-termini located cytoplasmically (Preston and Agre, 1991). *In vivo*, AQP1 assembles noncovalently into tetramers; however, each monomer is believed to be a functional water-passing unit (Smith and Agre, 1991; van Hoek et al., 1991).

One of the most problematic questions regarding AQP1 function has been the means by which it selectively passes water while excluding other small solutes and ions. X-ray crystallography of the channel points to some structural features that may help answer this question. The pore through AQP1 is very narrow, only about 4 angstroms in diameter. It is therefore small enough to act as a size-selective filter to exclude small solutes such as glycerol, ammonia, or urea (Ren et al., 2001). In addition, the pore is curvilinear,

bending ~25° as it passes through the membrane, and is lined with hydrophobic residues (Ren et al., 2001). These features create a condition in which a single polar water molecule must "ladder" through the pore by making sequential hydrogen bonds with each of the pore-lining residues, thus resulting in the exclusion of all ions, including H^+ and OH^-.

Although aquaporins are expressed widely throughout the body in many areas where water permeability is important to tissue function, the consensus in the field has been until recently that this family is not expressed in the nervous system. However, the discovery of AQP4 in astrocytic endfeet abutting capillaries (Nielsen et al., 1997) and of AQP9 in mitochondrial membranes in catecholaminergic neurons in the brain (Amiry-Moghaddam et al., 2005) has challenged this view. The work presented in this dissertation demonstrates that AQP1 is also expressed in the nervous system, in remarkably restricted sets of cells in the nociceptive and olfactory sensory systems.

Nociceptive Pathways

How does noxious stimulation in the periphery result in the conscious perception of pain? In the canonical view, specific receptors on the terminals of primary afferent nociceptors are activated, causing these cells to fire action potentials and communicate via synaptic neurotransmitter release with a second order neuron in the superficial dorsal horn of the spinal cord. These spinal cord neurons then send projections to areas of the brain implicated in pain sensation as well as integration of nociceptive input with processes involved in homeostasis and behavioral state. These areas include the

thalamus, parabrachial nucleus, periaqueductal grey, brainstem reticular formation, hypothalamus, and amygdala (Dostrovsky and Craig, 2006; Braz et al., 2005). From there, the nociceptive information is transferred to regions of the brain that subserve such complex functions as sensory discrimination and localization (somatosensory cortex), descending modulation of spinal inputs (rostral ventromedial medulla), and affective or motivational aspects of the pain experience (rostral anterior cingulate cortex). Since the first part of this dissertation is concerned primarily with features of the most distal aspects of this circuit, a more detailed discussion of primary afferent nociceptors and the spinal cord dorsal horn follows.

Primary afferent nociceptors

Nociceptors are cells of the peripheral nervous system that are specialized to respond only to stimuli of sufficient intensity to cause actual or potential tissue damage, a feature that was first recognized by Sherrington 100 years ago (Sherrington, 1906). Among the many kinds of sensory neurons, nociceptors are unique in that they are able to detect each of the various energy forms (thermal, mechanical, chemical) that can cause tissue damage; this is likely related to the crucial importance to the animal of sensing information about injury.

Nociceptors can be classified according to their electrophysiological and neurochemical properties. Generally, nociceptive nerve fibers are defined as belonging to the Aδ class if they have a conduction velocity > 2 m/s (consistent with myelination) or as C fibers if their conduction velocity is < 2 m/s (considered to be unmyelinated) (Meyer et al., 2006). Because of their

different conduction velocities, Aδ fibers are thought to underlie "first pain" and C fibers "second pain" that is experienced after very intense stimulation (Fields, 1987). Additionally, C fiber nociceptors can be further subdivided based on the neurochemical markers they express. It is traditionally recognized that there are two broad classes of DRG neurons that give rise to unmyelinated C fibers, a "non-peptidergic" class that binds the lectin IB4 and expresses the neurotrophin receptor Ret, and a "peptidergic" class that expresses such neuropeptides as substance P (SP) and calcitonin gene-related peptide (CGRP) as well as the high affinity nerve growth factor receptor trkA (Snider and McMahon, 1998). However, the division of these cells into just two classes is clearly an oversimplification since many molecules important to nociceptive function are expressed in subsets of DRG neurons that blur the traditional peptidergic/non-peptidergic definition, adding a dimension of complexity and diversity to the population of primary afferent nociceptors. Some examples of such molecules include the capsaicin receptor TRPV1 (Caterina et al., 1997), the 5-HT_{1D} and 5-HT_3 subtypes of serotonin receptors (Potrebic et al., 2003; Zeitz et al., 2002), the cytoskeletal protein peripherin (Parysek and Goldman, 1988), and the sensory neuron specific voltage-gated sodium channels $Na_v1.8$ and $Na_v1.9$ (Djouhri et al., 2003; Amaya et al., 2000).

The spinal cord dorsal horn

Primary afferent nociceptors send an axon branch into the dorsal horn of the spinal cord, making the first synaptic contact in ascending pathways that relay information about noxious stimuli in the periphery to the central nervous system.

The spinal cord is classically divided into ten laminae based on cytoarchitectonic features such as size and packing density of the neurons in each region (Rexed, 1952). Laminae I and II are the major targets for nociceptive primary afferent input. Lamina I makes up a thin veil of cells forming the most dorsal aspect of the spinal grey matter and contains both projection neurons (5%) and interneurons (95%) (Nandi et al., 1993; Bice and Beal, 1997a, b). This region receives input from Aδ afferents and some peptidergic C fibers. While most of the input into lamina I is of a nociceptive nature, it also receives information related to innocuous cooling, itch, and joint position (Willis and Coggeshall, 1991).

Lamina II is also known as the substantia gelatinosa based on its translucent appearance, which is due to a high density of small neurons as well as the absence of myelinated axons in this region. Lamina II can be further subdivided into outer and inner portions (IIo and IIi, respectively). Aδ and peptidergic C fibers synapse in lamina IIo and as such it receives predominantly nociceptive input. Lamina IIi, however, is innervated by the non-peptidergic class of C fiber nociceptors (Willis and Coggeshall, 1991). The distinct termination patterns of the peptidergic and non-peptidergic C fibers constitutes one of the most compelling facts arguing for differential functions of the two classes of C fiber afferents.

In contrast to the more superficial laminae, laminae III and IV receive inputs from low threshold mechanoreceptors. They are thus not considered to participate in normal transmission of nociceptive signals but rather to underlie innocuous light touch sensations.

Many lamina V neurons respond with graded activity when probed with stimuli of increasing intensity and are therefore known as wide dynamic range cells. This electrophysiological response indicates that they receive innervation conveying signals about both noxious and innocuous stimulation. The source of the non-nociceptive input is likely direct, via Aβ afferents, but the nociceptive input can be either direct, through innervation by Aδ fibers, or indirect, as lamina V is known to receive prominent polysynaptic innervation from lamina II (Willis and Coggeshall, 1991). As in lamina I, many lamina V cells are projection neurons that send axons to various brain regions.

Changes in nociceptive processing associated with injury

Changes associated with tissue injury

After damage to tissue occurs, the peripheral sensory nervous system shifts from functioning solely to detect changes in the animal's environment to serving as a means of protecting the injured area from further damage. Accompanying this shift are various changes in the functionality of nociceptors and nociceptive circuitry, including both a decrease in activation threshold and efferent actions on cutaneous tissue (Jänig and Levine, 2006). In addition, the contents of damaged cells spread throughout their surroundings and many of these, including ATP, protons, and arachidonic acid metabolites, can directly excite nociceptors (Julius and Basbaum, 2001). In a typical scenario, tissue damage would result in extrusion of these algogenic substances and consequent activation of nociceptors, which would in turn lead to release of chemical modulators from both the central and peripheral terminals of the nociceptor. Some of these modulators, including SP and CGRP, apart from

their role in neurotransmission can also act on blood vessels to induce vasodilation and extravasation of plasma proteins into the interstitial space (Haass and Skofitsch, 1985). These latter actions serve to establish a state of inflammation in the injured area. Additionally, an altered pain state is induced under these circumstances in which stimuli that are normally perceived as innocuous take on a painful quality (allodynia) and stronger stimuli that normally induce mild pain become intensely painful (hyperalgesia) (Cervero and Laird, 1996).

Because of increased or persistent peripheral activation, the dorsal horn of the spinal cord can also undergo long-term functional changes. Indeed, many clinical chronic pain cases are likely to be a manifestation of such long-term spinal reorganization. This plasticity, known as central sensitization, is characterized by a reduction in threshold of second-order neurons, increased spontaneous activity, and expansion of receptive field size (Woolf, 1983). On a molecular level, many of the same changes have been shown to occur in central sensitization as occur in long-term potentiation. It is thus implied that central sensitization may be a form of "molecular memory" in the spinal cord (Woolf and Salter, 2000).

Changes associated with nerve injury

Injury to a peripheral nerve, either through trauma or due to an underlying disease state such as diabetes, in many cases results in neuropathic pain. In contrast to normal acute or tissue injury-induced pain, neuropathic pain is pathophysiological and maladaptive: pain signals no longer represent

actual or potential tissue damage but rather reflect a malfunctioning nervous system.

Neuropathic pain is characterized by spontaneous activity of injured and adjacent intact peripheral axons, changes in expression of various molecules related to nociception, and central changes in sensory processing that result from these peripheral phenomena (Devor, 2006).

Several animal models have been developed to facilitate study of this condition, each of which involves damage to a major peripheral nerve and recapitulates the allodynia and hyperalgesia seen in clinical patients. Among the most commonly used of these are (1) chronic constriction injury, in which loose ligatures tied around the sciatic nerve trunk result in intraneural edema and demyelination; (2) partial sciatic ligation, which is performed by tightly ligating 1/3 to 1/2 of the sciatic nerve trunk; and (3) spinal nerve ligation, which involves ligation of the L5 (and sometimes L6) spinal nerve and allows investigation of the differential contributions of injured (L5) and intact (L4) neurons that contribute axons to the sciatic nerve (Bennett and Xie, 1988; Seltzer et al., 1990; Kim and Chung, 1992). Chapter 2 of the present work characterizes a new experimental model of neuropathic pain in the mouse, the spared nerve injury model, that has the advantage of being highly reproducible between subjects while being technically easy to perform.

References

Agre P, King LS, Yasui M, Guggino WB, Ottersen OP, Fujiyoshi Y, Engel A, Nielsen S (2002) Aquaporin water channels--from atomic structure to clinical medicine. J Physiol 542:3-16.

Amaya F, Decosterd I, Samad TA, Plumpton C, Tate S, Mannion RJ, Costigan M, Woolf CJ (2000) Diversity of expression of the sensory neuron-specific TTX-resistant voltage-gated sodium ion channels SNS and SNS2. Mol Cell Neurosci 15:331-342.

Amiry-Moghaddam M, Lindland H, Zelenin S, Roberg BA, Gundersen BB, Petersen P, Rinvik E, Torgner IA, Ottersen OP (2005) Brain mitochondria contain aquaporin water channels: evidence for the expression of a short AQP9 isoform in the inner mitochondrial membrane. Faseb J 19:1459-1467.

Bennett GJ, Xie YK (1988) A peripheral mononeuropathy in rat that produces disorders of pain sensation like those seen in man. Pain 33:87-107.

Bice TN, Beal JA (1997a) Quantitative and neurogenic analysis of neurons with supraspinal projections in the superficial dorsal horn of the rat lumbar spinal cord. J Comp Neurol 388:565-574.

Bice TN, Beal JA (1997b) Quantitative and neurogenic analysis of the total population and subpopulations of neurons defined by axon projection in the superficial dorsal horn of the rat lumbar spinal cord. J Comp Neurol 388:550-564.

Braz JM, Nassar MA, Wood JN, Basbaum AI (2005) Parallel "pain" pathways arise from subpopulations of primary afferent nociceptor. Neuron 47:787-793.

Castle NA (2005) Aquaporins as targets for drug discovery. Drug Discov Today 10:485-493.

Caterina MJ, Schumacher MA, Tominaga M, Rosen TA, Levine JD, Julius D (1997) The capsaicin receptor: a heat-activated ion channel in the pain pathway. Nature 389:816-824.

Cervero F, Laird JM (1996) Mechanisms of touch-evoked pain (allodynia): a new model. Pain 68:13-23.

Devor M (2006) Response of nerves to injury in relation to neuropathic pain. In: Textbook of Pain, Fifth Edition (McMahon SB, Koltzenburg M, eds), pp 905-927: Elsevier.

Djouhri L, Fang X, Okuse K, Wood JN, Berry CM, Lawson SN (2003) The TTX-resistant sodium channel Nav1.8 (SNS/PN3): expression and correlation with membrane properties in rat nociceptive primary afferent neurons. J Physiol 550:739-752.

Dostrovsky JO, Craig AD (2006) Ascending projection systems. In: Textbook of Pain, Fifth Edition (McMahon SB, Koltzenburg M, eds), pp 187-203: Elsevier.

Fields HL (1987) Pain. New York: McGraw-Hill.

Haass M, Skofitsch G (1985) Cardiovascular effects of calcitonin gene-related peptide in the pithed rat: comparison with substance P. Life Sci 37:2085-2090.

Jänig W, Levine JD (2006) Autonomic-endocrine-immune interactions in acute and chronic pain. In: Textbook of Pain, Fifth Edition (McMahon SB, Koltzenburg M, eds), pp 205-218: Elsevier.

Julius D, Basbaum AI (2001) Molecular mechanisms of nociception. Nature 413:203-210.

Kim SH, Chung JM (1992) An experimental model for peripheral neuropathy produced by segmental spinal nerve ligation in the rat. Pain 50:355-363.

Meyer RA, Ringkamp M, Campbell JN, Raja SN (2006) Peripheral mechanisms of cutaneous nociception. In: Textbook of Pain, Fifth Edition (McMahon SB, Koltzenburg M, eds), pp 3-34: Elsevier.

Nandi KN, Knight DS, Beal JA (1993) Spinal neurogenesis and axon projection: a correlative study in the rat. J Comp Neurol 328:252-262.

Nielsen S, Nagelhus EA, Amiry-Moghaddam M, Bourque C, Agre P, Ottersen OP (1997) Specialized membrane domains for water transport in glial cells: high-resolution immunogold cytochemistry of aquaporin-4 in rat brain. J Neurosci 17:171-180.

Parysek LM, Goldman RD (1988) Distribution of a novel 57 kDa intermediate filament (IF) protein in the nervous system. J Neurosci 8:555-563.

Potrebic S, Ahn AH, Skinner K, Fields HL, Basbaum AI (2003) Peptidergic nociceptors of both trigeminal and dorsal root ganglia express serotonin 1D receptors: implications for the selective antimigraine action of triptans. J Neurosci 23:10988-10997.

Preston GM, Agre P (1991) Isolation of the cDNA for erythrocyte integral membrane protein of 28 kilodaltons: member of an ancient channel family. Proc Natl Acad Sci U S A 88:11110-11114.

Ren G, Reddy VS, Cheng A, Melnyk P, Mitra AK (2001) Visualization of a water-selective pore by electron crystallography in vitreous ice. Proc Natl Acad Sci U S A 98:1398-1403.

Rexed B (1952) The cytoarchitectonic organization of the spinal cord in the cat. J Comp Neurol 96:414-495.

Seltzer Z, Dubner R, Shir Y (1990) A novel behavioral model of neuropathic pain disorders produced in rats by partial sciatic nerve injury. Pain 43:205-218.

Sherrington CS (1906) The integrative action of the nervous system. New York: Scribner.

Smith BL, Agre P (1991) Erythrocyte Mr 28,000 transmembrane protein exists as a multisubunit oligomer similar to channel proteins. J Biol Chem 266:6407-6415.

Snider WD, McMahon SB (1998) Tackling pain at the source: new ideas about nociceptors. Neuron 20:629-632.

van Hoek AN, Hom ML, Luthjens LH, de Jong MD, Dempster JA, van Os CH (1991) Functional unit of 30 kDa for proximal tubule water channels as revealed by radiation inactivation. J Biol Chem 266:16633-16635.

Willis WD, Coggeshall RE (1991) Sensory mechanisms of the spinal cord, Second Edition. New York: Plenum Press.

Woolf CJ (1983) Evidence for a central component of post-injury pain hypersensitivity. Nature 306:686-688.

Woolf CJ, Salter MW (2000) Neuronal plasticity: increasing the gain in pain. Science 288:1765-1769.

Zeitz KP, Guy N, Malmberg AB, Dirajlal S, Martin WJ, Sun L, Bonhaus DW, Stucky CL, Julius D, Basbaum AI (2002) The 5-HT3 subtype of serotonin receptor contributes to nociceptive processing via a novel subset of myelinated and unmyelinated nociceptors. J Neurosci 22:1010-1019.

Chapter 2

Spared nerve injury model of neuropathic pain in the mouse: A behavioral and anatomical analysis

Shannon D. Shields, William A. Eckert III and Allan I. Basbaum

Departments of Anatomy and Physiology and W.M. Keck Foundation Center for Integrative Neuroscience, University of California, San Francisco

Abstract

Mouse genetics has contributed significantly to our understanding of molecular mechanisms underlying tissue and nerve injury-induced persistent pain. To create a highly reproducible, relatively non-invasive model of neuropathic pain in the mouse, we examined the behavioral consequences of sparing each of the three distal branches of the sciatic nerve in wildtype mice, after a model originally described in the rat by Decosterd and Woolf (2000). Sparing the tibial branch, but sparing neither of the other branches, produced robust mechanical allodynia while leaving heat sensibility intact. To assess the topographic organization of the IB4 population of afferents from each branch and to compare anatomical consistency across injury models, we examined loss of thiamine monophosphatase (TMP) staining in the superficial dorsal horn after peripheral nerve injury. We found that each of the sciatic branches targets a distinct mediolateral location in inner lamina II and that each of the spared nerve injury models produced a more reproducible pattern of TMP staining loss than did partial tight ligation. These results improve upon previous nerve injury models in mouse, demonstrate similar behavioral changes as in rat, and provide novel information on the topographic organization of small diameter peripheral afferents in the mouse spinal cord.

Introduction

Neuropathic pain is a debilitating condition that often results from partial injury to a peripheral nerve. It is characterized by spontaneous pain, allodynia (pain produced by normally innocuous stimuli), and hyperalgesia (exaggerated response to noxious stimuli), and is often resistant to common therapeutic interventions (Koltzenburg and Scadding, 2001; Sindrup and Jensen, 1999; Woolf and Mannion, 1999). The development of animal models of nerve injury-induced pain has contributed significantly to the analysis of mechanisms that contribute to neuropathic pain syndromes. Most of these models have been developed in the rat, including sciatic nerve constriction (Bennett and Xie, 1988), spinal nerve ligation (Kim and Chung, 1992), and tight ligation of 1/3 to 1/2 of the sciatic nerve (Seltzer et al., 1990). Recently, Decosterd and Woolf (2000) developed a spared nerve injury (SNI) model, which is produced by complete transection of the common peroneal and tibial distal branches of the sciatic nerve, leaving the sural branch intact.

Because there is great interest in defining the molecules that contribute to the development of neuropathic pain, there is particular value to studying nerve injury-induced persistent pain in the mouse, an animal in which genetic studies are readily performed. To this end our laboratory previously adapted the Seltzer model of nerve injury to the mouse (Malmberg and Basbaum, 1998). The surgery is relatively easy to perform, but the model is characterized by considerable variability in the number and particular subsets of peripheral axons that are injured. Although adaptation of the spinal nerve ligation model to the mouse addresses the issue of variability, the surgical procedure is relatively difficult to perform and is highly invasive. In the present report, we

have adapted the SNI model of nerve injury-induced persistent pain to the mouse. The procedure is both reliable and easy to perform.

In addition to evaluating the behavioral consequences of sparing each of the three distal branches of the sciatic nerve, we examined the central termination of these branches by studying injury-induced changes in the pattern of thiamine monophosphatase (TMP) staining in the spinal cord dorsal horn. The enzyme TMP is expressed in cell bodies and central terminals of a subpopulation of small diameter dorsal root ganglion neurons that binds the lectin IB4 (Silverman and Kruger, 1990). Peripheral nerve injury results in transganglionic degenerative atrophy of the primary afferent terminals in the dorsal horn and consequent TMP staining loss (Knyihar-Csillik et al., 1986), permitting assessment of the topographic projection of the IB4-positive axons in the transected nerve branch. Finally, with a view to comparing results from different neuropathic pain models in the mouse, we also assessed the pain behavior and loss of TMP staining after SNI alongside these changes following partial nerve injury produced by partial tight ligation (Malmberg and Basbaum, 1998).

As in the rat, we find that each branch of the sciatic nerve has a distinct topographic projection to the superficial dorsal horn of the spinal cord. Sparing the tibial branch of the sciatic nerve (i.e., cutting the common peroneal and sural branches) produced the greatest and most reproducible reduction in nociceptive threshold. We find the SNI model in the mouse to be highly reproducible, with respect to both behavioral and anatomical changes. A preliminary report of these observations was published in abstract form (Shields et al., 2001).

Materials and Methods

All animal experiments were approved by the Institutional Animal Care and Use Committee of the University of California, San Francisco and were conducted in accordance with the National Institutes of Health Guide for the Care and Use of Laboratory Animals and the recommendations of the International Association for the Study of Pain.

Experiments were performed on 48 adult (20-25g) male C57BL/6 mice (Charles River) divided into 8 groups. One group underwent spared tibial injury under ketamine/xylazine anesthesia (n=5, see below). All other mice were operated under halothane anesthesia. Five groups were tested for behavioral effects on the medial plantar surface of the hindpaw: spared tibial injury (n=8), spared common peroneal injury (n=6), spared sural injury (n=6), partial tight ligation/Seltzer model (n=7), and sham surgery (n=6). The remaining two groups were tested on the lateral plantar surface of the hindpaw: spared sural injury (n=5) and sham surgery (n=5). Since the two sham groups were not found to differ statistically from each other, the data from these animals were pooled.

Nerve injury procedures

One group of animals was anesthetized with a mixture of ketamine and xylazine (60 mg/kg and 8 mg/kg, respectively). In all other animals, surgical procedures were performed under halothane anesthesia (1.75 to 2.5%). After skin and muscle incision, we tightly ligated two of the three terminal branches of the sciatic nerve (sural, tibial and common peroneal nerves; see Fig. 1) with

9-0 silk suture (Ethicon). Next, the ligated branches were transected distal to the ligature and ~2 mm of each distal nerve stump was removed. Caution was taken not to stretch or contact the intact, spared branch. In mice that underwent a Seltzer model procedure, we produced a partial nerve injury by tying a tight ligature with 9-0 silk suture around approximately 1/3 to 1/2 the diameter of the sciatic nerve (Malmberg and Basbaum, 1998; Seltzer et al., 1990). In sham controls the sciatic nerve and its branches were identically exposed but were neither ligated nor transected. In all animals, overlying muscle and skin layers were closed separately using 6-0 silk suture (Ethicon) and 7.5mm suture clips (Harvard Apparatus), respectively.

Behavioral testing

The experimenter who performed the behavioral tests was blind to the treatment group of the animals. On each test day we first habituated the mice to the test environment for at least 20 min.

To assess thermal sensitivity, we measured paw withdrawal latencies to a radiant heat stimulus (Hargreaves et al., 1988). Baseline and post-nerve injury paw withdrawal latencies were defined as the average of three measurements per paw taken at least 5 min apart. The stimulus intensity was adjusted to give a 10 sec baseline withdrawal latency. Cutoff in the absence of a response was 20 sec.

Mechanical sensitivity was assessed by placing animals on an elevated wire mesh grid and stimulating the hindpaw with von Frey hairs using the up-down paradigm (Chaplan et al., 1994). Behavioral testing took place on the day before surgery, as well as on days 1, 3, 7 and 14 after surgery.

Thiamine monophosphatase (TMP) histochemistry

Fourteen days after surgery, mice were deeply anesthetized with 100 mg/kg pentobarbital i.p. and transcardially perfused with 0.1M phosphate-buffered saline followed by a phosphate-buffered 10% formalin fixative. Spinal cords were removed, post-fixed for 4 h in the same fixative, and cryoprotected overnight in 30% sucrose. The L3-L6 segments of the spinal cords were individually sectioned in the transverse plane at a thickness of 40 µm on a freezing microtome.

Sections were washed in 0.04M Tris maleate buffer (pH 5.6), incubated for 90 min at 37°C in buffer containing 0.25% thiamine monophosphate chloride and 0.2% lead nitrate and developed for approximately 2 to 10 sec in 1% sodium sulfide, following a modified version of the protocol of Knyihar-Csillik et al. (1986). (All chemicals were from Sigma.) Reacted sections were mounted on gelatin-coated slides, air dried, dehydrated in ethanol, and coverslipped with DPX mounting medium (Electron Microscopy Sciences).

Densitometry

Densitometric analysis to quantify changes in TMP staining was done according to methods described in Abbadie et al. (1996). Briefly, we captured photomicrographs of the spinal cord (segments L4-L5) using a 4x objective and a CCD camera, then image analysis was performed with NIH Image software (http://rsb.info.nih.gov/nih-image/). The mediolateral length of lamina II was measured, then divided into thirds to define the medial, central and lateral divisions. We measured pixel density within each third for the

ipsilateral and contralateral sides of three sections per animal, using three animals per treatment group.

Statistical analysis

We used the following method to assess the effect of nerve injury on the response to mechanical and thermal stimuli over the two-week post-operative period. We compared responses for paw withdrawal latency (thermal) or 50% withdrawal thresholds (mechanical) of nerve-injured animals to those of sham-operated controls using repeated measures analysis of variance (ANOVA) followed by Fisher's protected least significant difference post hoc test. For clarity of presentation, the data are graphed as percent of baseline, where each animal is normalized to its own pre-surgery threshold value.

Results

General behavior

The general health of mice with nerve injuries did not differ from sham-operated controls or from untreated mice. Autotomy was never observed. In mice with a spared common peroneal nerve injury, we often observed a "foot drop". During locomotion, the injured hindpaw often dragged. When the mouse lifted the injured limb it appeared that the movement was a result of action at the hip, rather than at the knee or ankle.

Nociceptive threshold changes

In our initial analysis, we found that when the nerve injury was made in animals anesthetized with a ketamine/xylazine mixture, the mice never developed changes in mechanical threshold. This was true regardless of the SNI that was performed, even when the mice were tested for up to six weeks after the surgery (Fig. 2G and data not shown). Only when we switched to using halothane anesthesia during the nerve injury procedure did we observe significant changes in nociceptive threshold.

Spared tibial nerve injury resulted in a significant decrease in mechanical threshold compared to sham-operated mice (Fig. 2A; $p<0.05$). Mice with a spared tibial injury were observed to have a reduced threshold on each test day after injury throughout the duration of the experiment. Seltzer model injury also produced significant mechanical allodynia, of approximately the same magnitude and duration as spared tibial injury (Fig. 2C). By contrast, we did not find a significant mechanical allodynia in the other SNI variations (spared sural, measured either at the medial or lateral plantar surface of the hindpaw, Fig. 2D, F; spared common peroneal, Fig. 2B) or on the contralateral paw (not shown). Latency to respond to heat stimuli did not change following any of the SNI or Seltzer model treatments (Fig. 2H). Although a previous report in the rat found that SNI produces thermal hyperalgesia, described as an increased duration of withdrawal in response to a heat stimulus (Decosterd and Woolf, 2000), we never observed behavior indicative of a thermal hyperalgesic response.

Spinal termination of IB4 afferents

The pattern of TMP staining that we observed in unoperated mice is comparable to that reported previously in mouse (Akkina et al., 2001). The dense band of staining, which corresponds largely to the terminals of the IB4-positive primary afferent fibers, was concentrated in the inner part of lamina II (IIi). There was no change in sham-operated animals, which always showed dense TMP staining across the mediolateral extent of lamina IIi (Fig. 3A).

In a pilot study to determine the time course of loss of TMP staining after nerve injury, we transected the entire sciatic nerve and performed TMP histochemistry 2, 7, 14 or 21 days later. Figure 3B illustrates that complete sciatic nerve transection produced a marked decrease in staining in the medial two-thirds of the ipsilateral lamina IIi of the lumbar spinal cord dorsal horn at segments L4-L6. This pattern of sciatic nerve innervation is consistent with that observed in the rat; the most lateral segment of lamina IIi is innervated by the posterior cutaneous nerve (Swett and Woolf, 1985). Because the greatest decrease occurred 14 days post-injury, we chose this time point for all subsequent anatomical studies of the effects of partial nerve injury.

We observed distinct patterns of TMP loss in each of the SNI models. These patterns thus identified the zone of innervation in the dorsal horn of the spinal cord of each of the three sciatic nerve branches. For example, sparing the sural nerve resulted in loss of TMP staining in the medial third of lamina IIi (Fig. 3E); sparing the tibial (Fig. 3F) and common peroneal nerves (Fig. 3G) resulted in loss of staining in the central and lateral thirds, respectively, of the portion of lamina IIi innervated by the sciatic nerve. In contrast to the very consistent pattern of staining loss after SNI, we found

that the pattern of TMP staining loss after partial sciatic nerve injury in the Seltzer model was much more variable with respect to location of the terminal loss (Fig. 3C, D; Table 1). A summary of these data showing the innervation patterns of each of the three sciatic branches to lamina IIi is shown in Fig. 3H.

Discussion

In the present study, we demonstrate that spared nerve injury performed in mice produces robust and consistent changes in pain behavior. We observed a pronounced mechanical allodynia but the response to heat stimuli did not change. These observations in mouse are comparable, but not identical, to those reported for the SNI model in rat (Decosterd and Woolf, 2000), wherein mechanical allodynia and thermal hyperalgesia, but not thermal allodynia, were observed. We find that, in mice, sparing the tibial branch of the sciatic nerve (by cutting the common peroneal and sural branches), rather than sparing the sural branch as in the rat model, produces the most robust and consistent reduction of nociceptive threshold (Fig. 2A). We also document the distinct mediolateral topographic organization of the spinal projections of IB4-positive primary afferents from each of the three sciatic nerve branches. We conclude that spared tibial nerve injury is a very useful and reliable model of nerve injury-induced neuropathic pain with regard to behavioral measures, and that it produces a more consistent pattern of anatomical changes than another widely used model, partial tight ligation.

As we previously reported using the Seltzer model in the mouse (Malmberg and Basbaum, 1998), we find that the onset of the lowered mechanical threshold in the mouse spared tibial model is very rapid, peaking

within 3 days and lasting throughout the 14-day period of testing. Interestingly, we observed that when injuries were produced using ketamine/xylazine anesthesia, mechanical thresholds did not change following any of the three SNI models. This presumably reflects the fact that ketamine has antagonist properties at the N-methyl-D-aspartate (NMDA) receptor. This conclusion is consistent with numerous reports from studies using other nerve injury models (Kim et al., 1997; Munglani et al., 1999; Smith et al., 1994) that indicate that the mechanical threshold changes produced in such partial nerve injury models are NMDA-dependent and likely involve central sensitization.

Because pressing downward on the dorsal paw with a mechanical stimulus might limit the animal's ability to withdraw the paw from the stimulus, we focused our efforts on developing a mouse SNI model that could be tested from the plantar side of the paw. Since the common peroneal branch innervates the medial part of the dorsal hindpaw, sparing this nerve should effectively denervate the plantar surface of the paw. Our observation of an increased mechanical threshold in the spared common peroneal model is thus likely explained by the peripheral innervation pattern of this nerve.

Although sparing the sural branch leaves the innervation of a region of the plantar paw intact and readily testable, we unexpectedly also observed an increase rather than a decrease in mechanical threshold in this model, independent of whether the stimulus was applied to the medial or lateral portion of the plantar surface of the paw. This is perhaps due to the extremely small size of the sural nerve in mice, which increases the likelihood that a small, inadvertent mechanical disturbance during surgery damages a greater

proportion of axons in the sural nerve compared to the others. By contrast, the tibial nerve is the largest and best-protected branch of the sciatic nerve. This is particularly true when the surgery is performed from a lateral approach. Sparing the tibial branch thus leaves the medial plantar innervation intact, while denervating the lateral paw (both dorsal and plantar) and the medial dorsal paw. Taken together, these results argue for the use of the spared tibial model in the mouse and explain why this particular model displayed the most robust reduction in mechanical threshold of the three SNI models.

Although thermal thresholds are lowered in most animal models of nerve injury, this is not always a feature of clinical neuropathic pain (Koltzenburg, 1998). Consistent with the SNI model in rat, but in contrast to our group's previous report that adapted the tight ligation model to mouse, in the present study thermal thresholds did not change following injury in any of the SNI models or even after partial tight ligation. The fact that the partial tight ligation model did not produce allodynia to heat stimuli in the present study, but did in our previous study (Malmberg and Basbaum, 1998), may reflect the fact that producing injury in a variable number of axons and to different subsets of axons from a given nerve can lead to variable behavioral consequences.

Because the TMP enzyme is expressed exclusively in the IB4 population of primary afferents, we used TMP staining loss as a marker of central terminals of the specific population of IB4 axons that were injured. This allowed us to evaluate the somatotopic organization in the superficial dorsal horn of the IB4 terminals that derive from axons of each of the three

branches of the sciatic nerve, as well as to provide an anatomical correlate of the variability within and between injury models. Based on the pattern of TMP loss, we conclude that each of the three branches of the sciatic nerve has a distinct mediolateral projection to lamina IIi (Fig. 3H). Finally, we found that while tight ligation of a portion of the sciatic nerve produced a highly variable pattern of TMP staining loss, reflecting damage to different subsets and numbers of axons for each animal, each of the SNI models produced a highly reproducible pattern of TMP staining loss.

Interestingly, the maximal loss of TMP staining (at two weeks following injury) did not coincide with the onset or peak of the behavioral effects (one to three days post-injury). Clearly, the time course for the changes that initiate the behavioral sensitization is shorter than the time course for transganglionic degenerative atrophy of the nerve terminals. It follows that terminal atrophy is probably not required for the induction or expression of neuropathic pain syndromes.

There is evidence that the IB4-binding population of primary afferents is of particular importance to the development of nerve injury-induced neuropathic pain. It has been found that mechanical allodynia is significantly reduced following nerve injury when the IB4 population of primary afferent neurons is deleted using IB4 conjugated to the toxin saporin (Tarpley et al., 2002). Also, intrathecal injection of glial-derived neurotrophic factor (GDNF), a neurotrophin that supports survival of the IB4 population of C fibers, can prevent nerve injury-induced neuropathic pain conditions (Boucher et al., 2000).

In conclusion, the SNI model in the mouse, particularly the spared tibial nerve injury model, produces robust, apparently NMDA-dependent mechanical allodynia, which is accompanied by consistent changes in primary afferent terminal staining in the spinal cord. In addition, we demonstrate that the IB4 population of primary afferent terminals that derives from each of the three branches of the sciatic nerve in mouse terminates in distinct mediolateral regions of lamina IIi. Because the SNI model is easy to perform in the mouse, is relatively non-invasive and improves upon the reproducibility of mouse neuropathic pain models, we suggest that this model provides an extremely useful tool for the study of the development and maintenance of nerve injury-induced neuropathic pain in mice with specific gene deletions.

References

Abbadie C, Brown J, Mantyh P, Basbaum A (1996) Spinal cord substance P receptor immunoreactivity increases in both inflammatory and nerve injury models of persistent pain. Neuroscience 70:201-209.

Akkina S, Patterson C, Wright D (2001) GDNF rescues nonpeptidergic unmyelinated primary afferents in streptozotocin-treated diabetic mice. Exp Neurol 167:173-182.

Bennett G, Xie Y (1988) A peripheral mononeuropathy in rat that produces disorders of pain sensation like those seen in man. Pain 33:87-107.

Boucher T, Okuse K, Bennett D, Munson J, Wood J, McMahon S (2000) Potent analgesic effects of GDNF in neuropathic pain states. Science 290:124-127.

Chaplan S, Bach F, Pogrel J, Chung J, Yaksh T (1994) Quantitative assessment of tactile allodynia in the rat paw. J Neurosci Methods 53:55-63.

Decosterd I, Woolf C (2000) Spared nerve injury: an animal model of persistent peripheral neuropathic pain. Pain 87:149-158.

Hargreaves K, Dubner R, Brown F, Flores C, Joris J (1988) A new and sensitive method for measuring thermal nociception in cutaneous hyperalgesia. Pain 32:77-88.

Kim S, Chung J (1992) An experimental model for peripheral neuropathy produced by segmental spinal nerve ligation in the rat. Pain 50: 355-363.

Kim Y, Na H, Yoon Y, Han H, Ko K, Hong S (1997) NMDA receptors are important for both mechanical and thermal allodynia from peripheral nerve injury in rats. Neuroreport 8:2149-2153.

Knyihar-Csillik E, Bezzegh A, Boti S, Csillik B (1986) Thiamine monophosphatase: a genuine marker for transganglionic regulation of primary sensory neurons. J Histochem Cytochem 34:363-371.

Koltzenburg M (1998) Painful neuropathies. Curr Opin Neurol 11:515-521.

Koltzenburg M, Scadding J (2001) Neuropathic pain. Curr Opin Neurol 14:641-647.

Malmberg A, Basbaum A (1998) Partial sciatic nerve injury in the mouse as a model of neuropathic pain: behavioral and neuroanatomical correlates. Pain 76:215-222.

Munglani R, Hudspith M, Fleming B, Harrisson S, Smith G, Bountra C, Elliot P, Birch P, Hunt S (1999) Effect of pre-emptive NMDA antagonist treatment on long-term Fos expression and hyperalgesia in a model of chronic neuropathic pain. Brain Res 822:210-219.

Seltzer Z, Dubner R, Shir Y (1990) A novel behavioral model of neuropathic pain disorders produced in rats by partial sciatic nerve injury. Pain 43:205-218.

Shields S, Eckert W, Basbaum A (2001) Neuropathic pain models and somatotopy of primary afferents in the mouse. Soc Neurosci Abstr 27:283.18.

Silverman J, Kruger L (1990) Selective neuronal glycoconjugate expression in sensory and autonomic ganglia: relation of lectin reactivity to peptide and enzyme markers. J Neurocytol 19:789-801.

Sindrup S, Jensen T (1999) Efficacy of pharmacological treatments of neuropathic pain: an update and effect related to mechanism of drug action. Pain 83:389-400.

Smith G, Wiseman J, Harrison S, Elliott P, Birch P (1994) Pre treatment with MK-801, a non-competitive NMDA antagonist, prevents development of mechanical hyperalgesia in a rat model of chronic neuropathy, but not in a model of chronic inflammation. Neurosci Lett 165:79-83.

Swett J, Woolf C (1985) The somatotopic organization of primary afferent terminals in the superficial laminae of the dorsal horn of the rat spinal cord. J Comp Neurol 231:66-77.

Tarpley J, MacIntyre E, Martin W (2002) Loss of IB4-positive sensory neurons mitigates the consequences of nerve injury in the rat. IASP Abstracts 1136-P52.

Woolf C, Mannion R (1999) Neuropathic pain: aetiology, symptoms, mechanisms, and management. Lancet 353:1959-1964.

Figure 1. Layout of sciatic nerve and its branches, including manipulations performed for Seltzer and SNI models of neuropathic pain. The common peroneal, tibial, and sural nerves are the three distal branches of the sciatic nerve; two of the three are ligated and cut in the SNI model. Partial tight ligation, or Seltzer model, is performed more proximally and involves tying off 1/3 to 1/2 of the sciatic nerve.

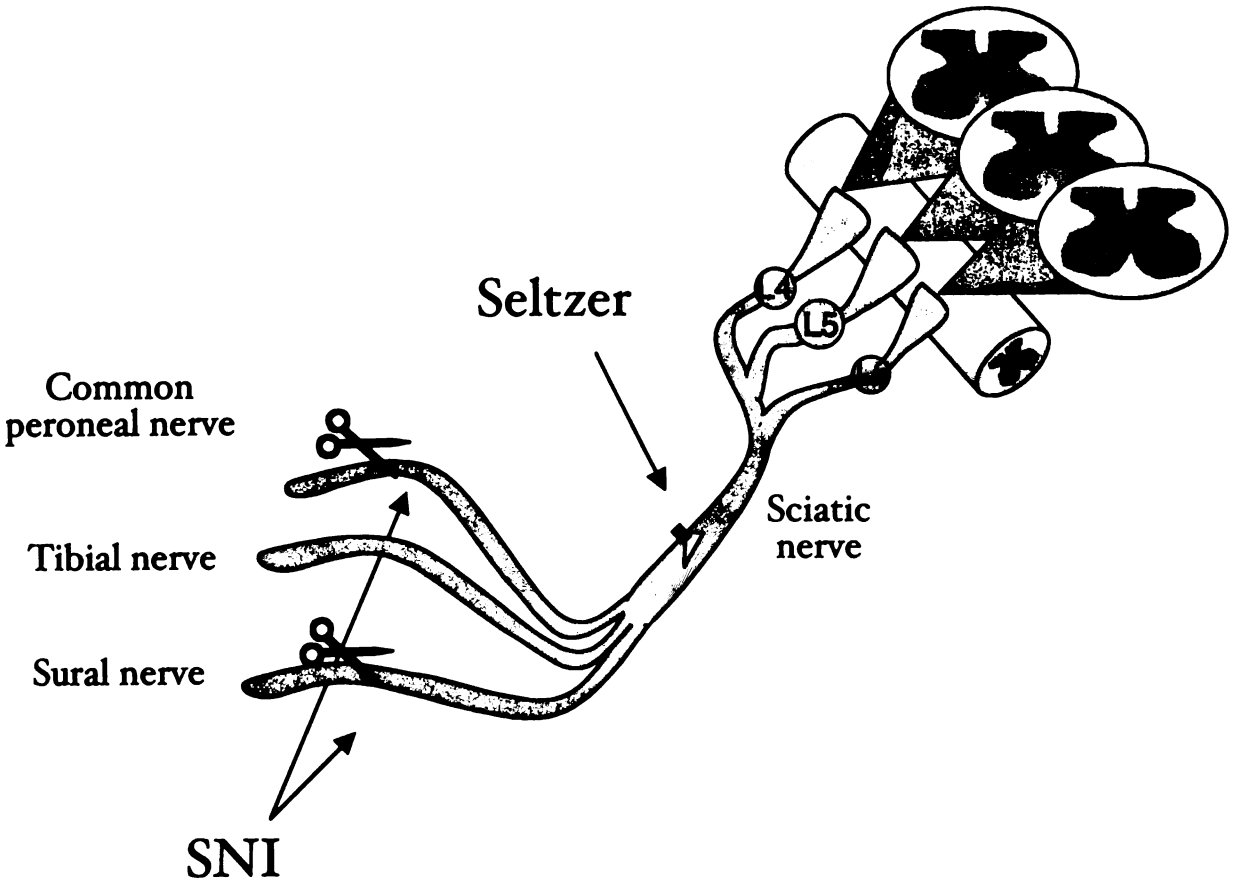
Seltzer
L4
L5
Common
peroneal nerve
Tibial nerve
Sural nerve
Sciatic
nerve
SNI

Figure 2. Behavioral assessment of mechanical and thermal responsiveness in the different nerve injury models. (A-F) Mechanical threshold changes following nerve injury, reported as percent of pre-surgery baseline ± SEM. Spared tibial nerve injury (A) and Seltzer model injury (C), but none of the other SNI models (B,D,F), produced a significant mechanical allodynia compared to sham (E; $p<0.05$, repeated measures ANOVA). (G) When ketamine (60 mg/kg, i.p.) was included in the anesthetic mixture, changes in mechanical threshold were not observed following spared tibial injury. (H) Paw withdrawal latency to thermal stimulation is unchanged following any of the nerve injury models tested. Solid black line, spared sural nerve injury; long dashes, Seltzer model; medium dashes, spared tibial nerve injury; short dashes, spared common peroneal nerve injury; dotted line, sham. Note that y-axes are scaled differently for some panels. The dashed lines in A-G represent the baseline thresholds, against which percent changes were determined.

A. Spared Tibial Nerve

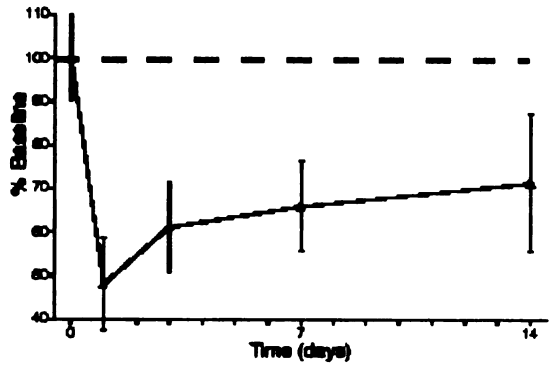

B. Spared Common Peroneal Nerve

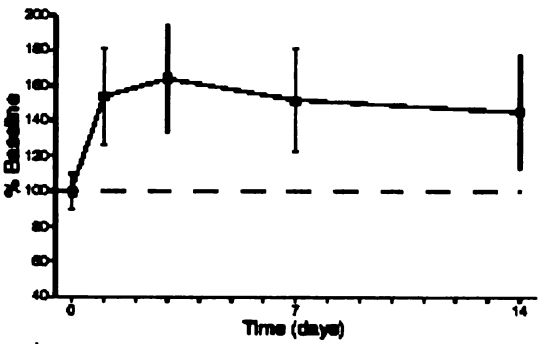

C. Seltzer Model

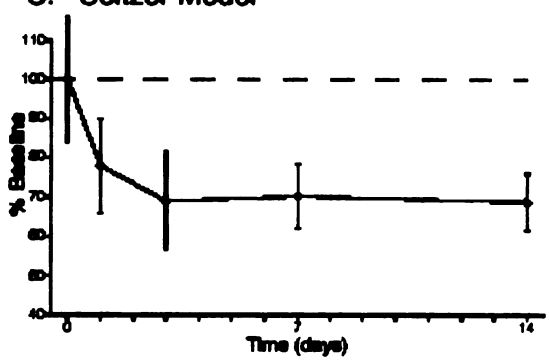

D. Spared Sural Nerve (Lateral Plantar Surface)

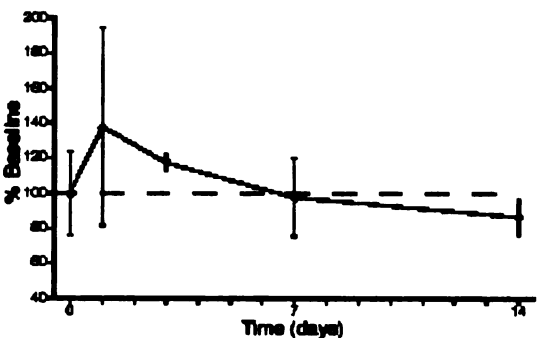

E. Sham Surgery

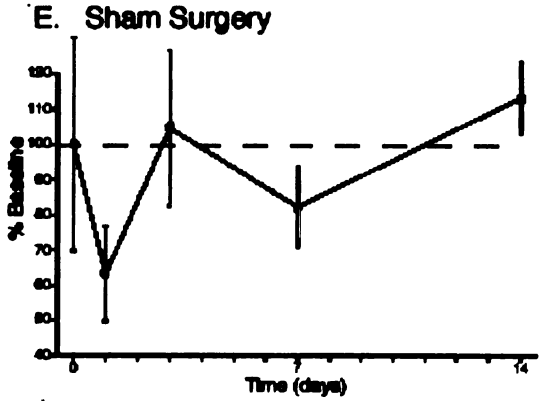

F. Spared Sural Nerve (Medial Plantar Surface)

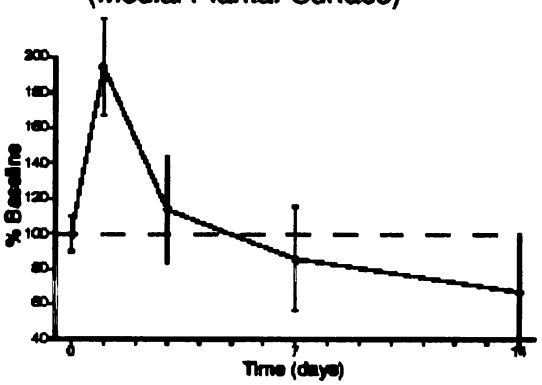

G. Spared Tibial Nerve, Ketamine Anesthesia

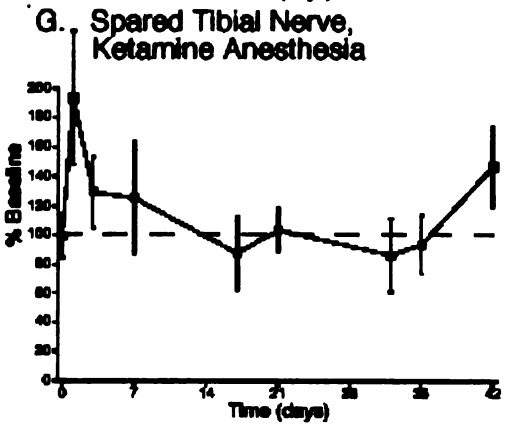

H. Thermal Thresholds

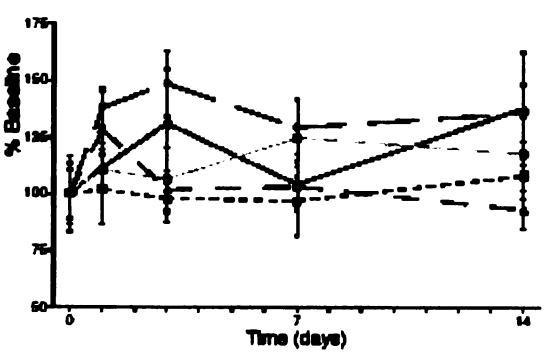

Figure 3. Loss of TMP staining in central terminals of injured primary afferents reveals somatotopic organization of spared afferent inputs to the superficial laminae of the lumbar spinal cord. Representative sections of L_4-L_5 from each of the injury models are shown. (A) Sham-operated animals show dense staining across the entire mediolateral extent of lamina IIi. (B) Complete transection of the sciatic nerve results in TMP staining loss in the medial two thirds of lamina IIi. The persistent staining derives from afferents in the posterior cutaneous nerve. (C) and (D) are two examples of animals with Seltzer model injury. Note the variability in location and magnitude of TMP staining loss. (E) Sparing the sural nerve results in preservation of TMP staining in the most lateral and central portions of lamina IIi innervated by the sciatic nerve. (F) Sparing the tibial nerve results in preservation of TMP staining in the most lateral and most medial portions of lamina IIi. (G) Sparing the common peroneal nerve results in preservation of TMP staining in the most medial and central portions of lamina IIi. Scale bar is the same for all photomicrographs and represents 200 μm. (H) Summary of termination patterns for each of the nerves that innervate lamina IIi.

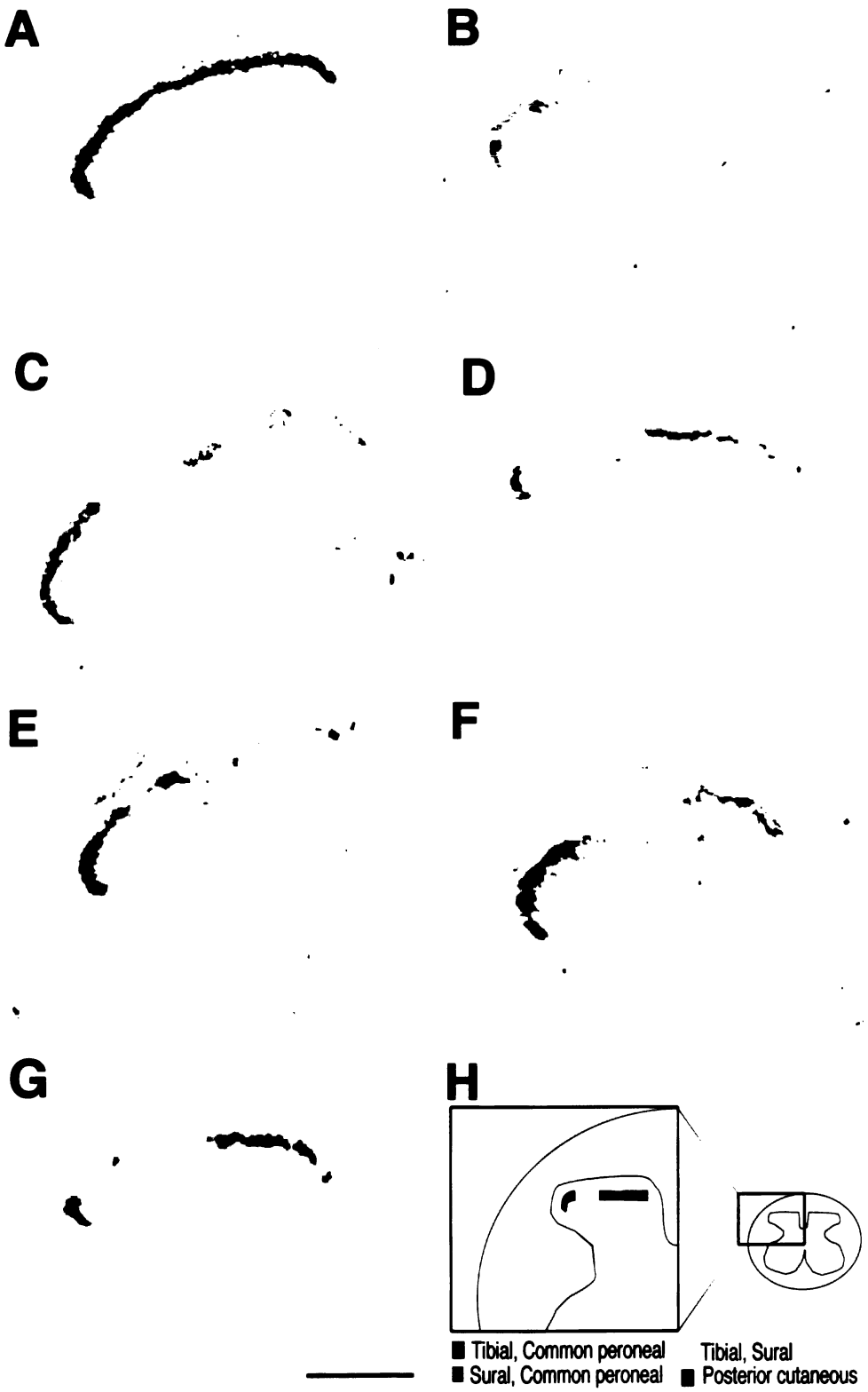
A
B
C
D
E
F
G
H
Tibial, Common peroneal
Sural, Common peroneal
Tibial, Sural
Posterior cutaneous

Table 1. Spared tibial injury results in a more consistent pattern of TMP staining loss than does Seltzer model injury.

	Mean density (% contralateral)	Standard deviation
Spared tibial injury		
Medial third	98.16	17.63
Central third	55.58	12.80
Lateral third	80.31	16.23
Seltzer model injury		
Medial third	77.23	16.49
Central third	71.73	29.34
Lateral third	64.98	23.08

Chapter 3

Anatomical and Functional Analysis of Aquaporin 1, a Water Channel in Primary Afferent Neurons

Shannon D. Shields, Javier Mazario, Kate Skinner, and Allan I. Basbaum

Depts. of Anatomy and Physiology and W. M. Keck Foundation Center for Integrative Neuroscience, University of California, San Francisco

Abstract

Aquaporin 1 (AQP1) is the archetypal member of a family of water channel proteins that contribute to water homeostasis in kidney, lung, and other tissues. Although there is limited evidence that aquaporins are expressed in the nervous system, AQP4 is expressed in glia and AQP9 is present on some neuronal and glial mitochondria. In the present study, we used immunohistochemistry to show that AQP1 is heavily and exclusively expressed in a population of small diameter primary sensory neurons of dorsal root, trigeminal, and nodose ganglia. AQP1 immunoreactivity is abundant in DRG cell bodies and in both the peripheral and central branches of primary afferent neurons, and colocalizes with markers of nociceptors, notably substance P and IB4. AQP1 expression in DRG is first detectable at embryonic day 15.5, which corresponds to the developmental stage when the majority of fine cutaneous afferents penetrate the superficial dorsal horn. Electron microscopic analysis revealed dense membrane labeling both of fine diameter myelinated and unmyelinated axons and of synaptic terminals in the superficial dorsal horn. Because this restricted and dense expression suggested that AQP1 contributes to nociceptive processing, we next studied behavioral responses of wildtype and AQP1 -/- mice in a comprehensive battery of acute and persistent pain tests. We also used *in vivo* electrophysiology to measure the responses of spinal lamina V wide dynamic range neurons in these animals to thermal stimulation before and after noxious stimulus-induced sensitization. To date we have not detected a differential phenotype suggestive of a functional contribution of AQP1 to nociceptive processing.

Introduction

The primary afferent nociceptor is the first site at which a noxious stimulus is transduced into a neural signal. There is remarkable molecular diversity of primary afferent sensory neurons which is manifest in their expression of a variety of neuropeptides, ion channels, G-protein coupled receptors, and other signaling molecules, some of which are exclusively expressed by these neurons. The discovery of such signaling components has contributed to a better understanding of the mechanisms underlying the transmission of nociceptive messages in normal and pathophysiological states, and has identified novel therapeutic targets for the treatment of pain. In this study we present the first comprehensive report of a very dense, but remarkably restricted expression of a member of the aquaporin family of water channels in primary afferent nociceptors.

The aquaporins comprise a large family of integral membrane proteins that function as water-selective channels in animals, plants, and microorganisms. To date, thirteen mammalian aquaporins have been identified (for review, see Castle, 2005). AQP1, the archetypal member of this family, is a constitutively open, bidirectional water channel expressed in red blood cells, renal proximal tubules, capillary endothelium, and other water permeable tissues (Agre et al., 2002). With the exception of abundant AQP1 expression in choroid plexus and a report of its expression in amacrine cells of the rat retina (Kim et al., 2002) this protein appears not to be expressed in brain, neither in glia nor in neurons.

In the present study we expand on our brief report of AQP1 expression in the superficial dorsal horn of the spinal cord (Shields et al., 2004) and

demonstrate that this water channel is, in fact, concentrated in neurochemically and neuroanatomically defined nociceptors of the mouse dorsal root and trigeminal ganglia. To determine whether AQP1 indeed contributes to nociceptive processing, we studied wildtype and AQP1 null mutant mice in a battery of electrophysiological and behavioral tests. Despite the remarkably localized and heavy expression of AQP1 in nociceptors, we have yet to uncover deficits in nociceptive processing in the absence of AQP1.

Materials and Methods

All animal experiments were approved by the Institutional Animal Care and Use Committee of the University of California at San Francisco and were conducted in accordance with the National Institutes of Health Guide for the Care and Use of Laboratory Animals and the recommendations of the International Association for the Study of Pain. AQP1 -/- mice (Ma et al., 1998) were generated in the laboratory of Drs. Alan Verkman and Geoffrey Manley (University of California, San Francisco) and were subsequently produced by interbreeding heterozygotes. Offspring were genotyped by polymerase chain reaction (primers to detect wildtype allele: 5'—tcagtggctaacaacaaacaggg—3' and 5'—cttcgtcttcatcagcattggttc—3'; primers to detect knockout allele: 5'—cacaagaactcgtcaagaagg—3' and 5'—atgggatcggccattgaacaa—3').

Light Microscopy

Tissue preparation. Adult mice (20-30g) were deeply anesthetized with 100 mg/kg sodium pentobarbital and perfused transcardially with 0.1M phosphate-

buffered saline (PBS) followed by 10% formalin in PBS. Spinal cords, dorsal root ganglia, trigeminal ganglia, nodose ganglia, superior cervical ganglia, and brains were collected, post-fixed in the same fixative for 4 hours, and cryoprotected overnight in 30% sucrose in 0.1M PBS. Spinal cords and brains were sectioned on a freezing microtome at 30-40 µm and processed as free-floating sections. Ganglia were cut at 12 µm on a cryostat and sections were processed on the slide. For bladder tissue processing, the bladder was removed after perfusion of PBS only, then stretched tightly on a piece of dental wax with fine metal pins before postfixing as above. Bladder tissue was then stained as a whole mount preparation.

To time embryo collection, we considered the morning of the day on which a vaginal plug was detected as embryonic day (E) 0.5. Embryos were removed individually and perfused transcardially (E15.5 and older) or immersion fixed with 4% paraformaldehyde. After removing viscera, embryos were embedded in M1 medium (Thermo Shandon, Pittsburgh, PA) and sectioned at 40 µm on a cryostat.

Immunohistochemistry. Primary antisera were as follows: rabbit anti-AQP1 (1:10,000; Chemicon Inc., Temecula, CA), guinea pig anti-substance P (1:600; gift from J. Maggio, University of Cincinnati, Cincinnati, OH), monoclonal anti-NF200 (clone N52; 1:1000; Sigma, St. Louis, MO), guinea pig anti-TRPV1 (1:600; gift from D. Julius, University of California at San Francisco, San Francisco, CA). Secondary antisera, all purchased from Jackson ImmunoResearch (West Grove, PA), were: Cy2-labeled anti-guinea pig IgG, anti-mouse IgG, (all 1:200), or Cy3-labeled anti-rabbit IgG (1:600).

Tissue was incubated for 1 hr in 0.1M PBS with 0.3% Triton X-100 (PBST) plus 5% normal goat serum (NGS). Primary and secondary antisera were diluted in PBST plus 1% NGS. Tissue was incubated overnight at room temperature in primary antibody solution. Between incubations, tissue was rinsed in 0.1M PBS plus 1% NGS. Tissue was then incubated with the appropriate secondary antiserum and washed in PBS. For double immunofluorescence, the process was repeated using the other primary and secondary antisera. Slides were coverslipped with DPX mounting medium (Electron Microscopy Sciences, Fort Washington, PA). For isolectin B4 (IB4) binding, we added biotinylated IB4 (1:500; Vector Laboratories, Burlingame, CA) instead of primary antiserum and followed this with Cy2-conjugated streptavidin (1:500; Jackson ImmunoResearch) instead of a secondary antiserum.

Digitized images were captured with a CCD camera attached to a BioRad 1024 confocal microscope (BioRad, Hercules, CA) and analyzed with Adobe Photoshop (Adobe Systems Inc., San Jose, CA). At least three DRG sections from no fewer than three mice were analyzed for quantification of the extent of double labeling. For densitometry measurements of changes in AQP1 expression levels after hindpaw injection of Complete Freund's Adjuvant (CFA; see below) or after transection of the sciatic nerve, we captured digitized images using a CCD camera attached to a Nikon Eclipse fluorescence microscope and analyzed the results using NIH Image software (http://rsb.info.nih.gov/nih-image). We measured pixel density within the

region of sciatic innervation and normalized to background by subtracting pixel density from an unstained region in the neck of the dorsal horn.

Electron microscopic immunohistochemistry

In our experience the fine structural quality of nervous system material is superior in the rat compared to the mouse, and thus we performed these experiments in rats. Two adult Sprague-Dawley rats were deeply anesthetized and perfused for electron microscopic immunohistochemistry, first with heparin saline and then with acrolein/paraformaldehyde or 2% formaldehyde/2% glutaraldehyde/0.2% picric acid in 0.1 M phosphate buffer (pH 7.4). Sagittal Vibratome sections (25 μm) of the lumbar spinal cord were processed for pre-embedding immunohistochemistry with primary antibody at 1:10,000 dilution. Some sections were treated with 50% ethanol for 30 minutes to improve penetration of antibodies. The immunohistochemical reaction was localized with 1.0 nm gold-conjugated secondary antibody, which was then silver-enhanced by standard methods (IntenSE, Amersham, Piscataway, NJ) to produce a particulate reaction product. Sections were osmicated, flat-embedded in Durcupan resin, thin-sectioned and counterstained with uranyl acetate and lead citrate before examination in a Jeol electron microscope.

In situ *hybridization*

Digoxygenin-labeled probes were transcribed from linearized pBluescript II SK vector (Stratagene, La Jolla, CA) containing a portion of the 3' untranslated region of the AQP1 cDNA. Hybridization was conducted

as described previously (Zeitz et al., 2002). The hybridized probe was visualized by incubation with alkaline phosphatase-linked anti-digoxygenin Fab fragments (Roche, Mannheim, Germany) followed by reaction with 4-nitro blue tetrazolium chloride and 5-bromo-4-chloro-3-indolylphosphate (Roche) according to the specifications of the manufacturer.

Spinal cord electrophysiology

Experiments were performed in AQP1 +/+ and -/- mice by an experimenter blind to genotype. Animals were anesthetized with 1.3 g/kg i.p. urethane (Sigma) and an i.p. cannula was implanted for administration of supplemental doses of anesthetic. Heart and breathing rates were monitored and used to indicate depth of anesthesia. To minimize spinal cord swelling, dexamethasone (0.2 mg, s.c.; American Regent Laboratories, Shirley, NY) was given prior to the beginning of surgery. Atropine (0.3 mg, s.c.; Sigma) was administered to reduce buildup of mucus in the airways. After laminectomy to expose the L4 and L5 segments of the spinal cord the dura was retracted and the vertebral segments rostral and caudal to the laminectomy clamped to suspend the animal so as to minimize movement of the spinal cord. A well surrounding the spinal cord was formed with agar and filled with mineral oil. The animal's core temperature was monitored with a rectal probe and maintained close to 37° C using a thermal pad and a feedback-controlled infrared lamp. The animals breathed spontaneously during the experiment.

We recorded extracellular potentials of wide dynamic range (WDR) neurons 400 to 650 μm from the surface of the spinal cord using a fine-tipped

tungsten microelectrode with an impedance of 10 MΩ at 1 kHz (FHC, Brunswick, ME). Data were acquired and processed using Micro1401 and Spike 2 software (CED, Cambridge, UK). Search stimuli for neurons consisted of applying soft pressure or brushing to the plantar surface of the paw. Once a neuron was isolated, we tested for its responses to brush, light pressure, or pinch. Only neurons that encoded these mechanical stimuli in a graded fashion were considered to be WDR. Thermal stimuli (40°, 45°, and 50° C) were then delivered via a 9 mm^2 copper probe heated and cooled by a 9W Peltier effect device with a rise rate of 2° C/s. The heat stimuli were applied for 10 seconds and separated by at least 1 minute. The thermal probe was maintained at 37° C between periods of stimulation. To activate large numbers of nociceptors, we applied mustard oil (MO; allyl isothiocyanate; Sigma) diluted to 10% with mineral oil (~60 µl) to the paw around the probe, and recorded the responses evoked for 10 minutes. Finally, to assess the magnitude of injury-induced sensitization produced by mustard oil, we retested the responsiveness of the neurons to the different thermal stimuli every 10 minutes after MO for 60 minutes.

Behavioral testing

All behavioral testing was performed blinded to genotype. Where applicable, animals were habituated to the test apparatus for 30-60 minutes prior to testing.

Hindpaw radiant heat (Hargreaves) test. Mice were placed in plastic chambers on a glass surface heated to 25°C through which a radiant heat source (Department of Anesthesiology, University of California at San Diego, La

Jolla, CA) was focused on the hindpaw. We recorded the latency to withdraw the paw and measured the average of three trials per animal taken ≥ 5 min apart. Cutoff to avoid tissue damage was 20 sec.

Tail flick test. Mice were lightly restrained as the tail was positioned over a radiant heat source (TechniLab Instruments, Pequannock, NJ). Latency to withdraw the tail was recorded and was measured as the average of five trials per animal taken ≥ 5 min apart. Cutoff latency was 10 sec.

Hot plate test. Mice were placed on a hot plate (Colombus Instruments, Columbus, OH) and latency to lick the hindpaws or to jump was recorded. This was measured as the average of three trials per animal taken ≥ 5 min apart. Cutoff latency was 1 min for 50 and 52.5°C or 30 sec for the 55°C stimulus.

von Frey test of mechanical threshold. Mice were placed in plastic chambers on a wire mesh grid and stimulated with von Frey filaments (North Coast Medical Inc., Morgan Hill, CA) according to the up-down method of Chaplan et al. (1994).

Formalin test. We made an intraplantar injection of 10 µl of 2% formalin in saline after which we recorded the time spent licking the injected hindpaw (in 5 min bins for 1 hr).

Capsaicin test. An intraplantar (i.pl.) injection of 3 µg capsaicin (Sigma) in a volume of 10 µl (vehicle: 10% ethanol, 0.5% Tween 80, and saline) was made and time spent licking the injected hindpaw was recorded during the first 5 min after injection. Paw edema was measured with a spring-loaded digital caliper (Mitutoyo, Kawasaki, Japan).

Complete Freund's Adjuvant (CFA) injection. We made an intraplantar (i.pl.) injection of 10 µl of a 1:1 saline/CFA (Sigma) emulsion and then tested thermal and mechanical thresholds daily as described above for one week. Paw edema was measured as above.

Spared nerve injury model of neuropathic pain. We performed the spared nerve injury surgery as described in Shields et al. (2003). Briefly, an incision was made in the thigh muscle and the common peroneal and sural nerves were ligated with 9-0 silk (Ethicon, Somerville, NJ) and transected, leaving the tibial nerve intact. The incision was then closed in two layers, using 6-0 silk (Ethicon) and 7.5 mm suture clips (Harvard Apparatus, Holliston, MA) for the muscle and skin, respectively. Mechanical threshold testing was performed as described above on days 1, 3, 7, and 14 after surgery.

Prostaglandin E2 (PGE2) inflammation and hypoosmotic challenge. PGE2 (100 ng in a volume of 2.5 µl; Sigma) was injected i.pl. Control animals received an equivalent volume injection of the vehicle (saline + 0.0008% Tween 20). Thirty min later, 10 µl of distilled H_2O was injected i.pl. and the number of flinches was recorded during the first 5 min after injection.

Plasma extravasation

Mice were anesthetized with 2% isoflurane throughout the duration of the experiment. Five min after i.v. injection of 2.5 ml/kg 2% Evans Blue dye (Sigma), we applied 12.5 µl of 10% mustard oil (Sigma) to each side of the ear. Thirty min later, the animals were killed by cervical dislocation and a 5 mm diameter skin punch was cut from the inflamed area. Skin punches were incubated overnight at 70°C in 1.0 ml formamide. To assay the amount of

extravasated dye, we measured optical density of the solution at 620 nm (OD620) using a spectrophotometer; results are reported in arbitrary units (A.U.).

Statistical analysis

Electrophysiological data were analyzed by two-way ANOVA followed by Newman-Keuls posthoc test for comparisons between genotypes over time, and by one-way ANOVA for comparisons within the same genotype. The depth of the recorded neurons was compared with Student's t-test. GBStat and GraphPad Prism software were used for the analysis. Statistical comparisons of mechanical thresholds were carried out using the non-parametric Friedman test, with comparisons between groups at individual time points made with the Mann-Whitney U-test. We compared thermal threshold changes over time after CFA injection using repeated measures ANOVA. For all other behavioral tests and for densitometry results, we used Student's unpaired t-test. In all cases, we considered a p-value of <0.05 to be the cutoff for statistical significance.

Results

Neuroanatomical distribution of AQP1

AQP1 expression in adult primary afferent neurons

The expression of AQP1 immunoreactivity in the nervous system is remarkably restricted. Dense AQP1-like immunoreactivity (IR) is present in Lissauer's tract and in laminae I and II of the spinal cord dorsal horn at all levels examined (Fig. 1A). Some fibers arborize ventrally, in the region of

lamina V and around the central canal. AQP1 IR is completely absent in the spinal cord of mice in which the AQP1 gene has been deleted (Fig. 1B), confirming the specificity of the antibody.

Because the observed pattern of staining is characteristic of the terminal distribution of primary afferent neurons, we focused our attention on AQP1 expression in the dorsal root ganglia (DRG). We found AQP1 IR in cell bodies of large numbers of small diameter neurons of both the DRG (Fig. 1C) and the trigeminal ganglia (data not shown), which contain cell bodies of primary afferents that innervate the head. These observations indicate that primary afferents are an important source of the spinal cord AQP1 IR, but do not rule out a possible expression in neurons intrinsic to the spinal cord. To address this question we used in situ hybridization to localize all neurons in which AQP1 is synthesized. As expected, we found that mRNA for AQP1 is concentrated in a subset of neuronal cell bodies in the DRG (Fig. 1D), but we never observed AQP1 mRNA in spinal cord neurons (Fig. 1E). Taken together, these data indicate that the spinal cord AQP1 derives exclusively from primary sensory neurons that target neurons in the superficial dorsal horn.

Ultrastructural localization of AQP1 in presynaptic axons and terminals of the spinal cord

In accordance with its function as a water channel, AQP1 is typically expressed on the surface of cells. However, given that its function in neurons is unknown, we next used electron microscopy to address the subcellular location of the channel. The light microscopic distribution of AQP1 IR in the rat did not differ from that observed in the mouse (data not shown) and thus

because of the superior fine structural quality of rat tissue, Sprague-Dawley rats were used instead of mice in this experiment. Figure 2 illustrates the striking subcellular localization of immunoreactive AQP1 in the superficial dorsal horn of the lumbar spinal cord. There is very dense AQP1 IR in patches along the plasma membrane of axons (Fig. 2A). The great majority of the labeling was associated with unmyelinated axons, but we did observe unmistakable immunostaining of a few myelinated axons (Fig. 2B). It is of interest that although AQP1 IR can also be seen along the membrane of synaptic terminals, the protein appears to be specifically excluded from the synaptic density (Fig. 2C).

AQP1 in the peripheral nervous system

We next investigated whether AQP1 protein is also transported to the peripheral branch of the primary afferent axons. In these studies we examined the bladder and found that AQP1 IR is abundant in what appear to be terminal arborizations of neurons (Fig. 1G). Because we find no evidence for AQP1 IR in motoneurons or in sympathetic postganglionic neurons (see below), we believe that the bladder staining represents the peripheral terminals of sensory neurons, supporting the hypothesis that AQP1 is present along both the central and peripheral branches of primary sensory neurons.

We next asked whether primary afferents from all body regions express AQP1 or if the neuronal expression of this channel is unique to DRG and trigeminal ganglia. The nodose ganglion contains cell bodies of primary afferent neurons that relay sensory signals from the viscera via the vagus nerve to the nucleus of the solitary tract (NTS) in the caudal medulla. We found

that a subset of neurons in the nodose ganglia indeed expresses AQP1 IR, and that terminal staining is also observed in the NTS (data not shown). By contrast, the superior cervical ganglion, which contains postganglionic sympathetic efferents, shows no neuronal AQP1 IR, although capillary endothelium within this ganglion did immunostain positively for AQP1 (data not shown). This is consistent with a previous report of AQP1 labeling in capillary endothelium in the peritoneum (Nielsen et al., 1993).

Neurochemical phenotype of AQP1 immunoreactive primary afferents

To further characterize the population of primary afferent neurons that expresses AQP1, we undertook double immunohistochemistry studies using markers that have been associated with subsets of primary afferent nociceptors (Snider and McMahon, 1998). AQP1 is highly concentrated in unmyelinated axons; this is confirmed by the minimal overlap of AQP1 IR with labeling for neurofilament 200, a marker of cell bodies with myelinated axons (Fig. 3A, B).

There are two broad classes of DRG neurons that give rise to unmyelinated C-fibers, a "non-peptidergic" class that binds the lectin IB4 and a "peptidergic" class that expresses a variety of neuropeptides, notably substance P and calcitonin gene-related peptide. Quantitative analysis of staining in these two populations indicates that 37 ± 2% of IB4-binding afferents (Fig. 3C, D) and 89 ± 7% of Substance P-positive afferents (Fig. 3E, F) co-express AQP1 IR. Of DRG cells immunoreactive for the capsaicin receptor TRPV1, 70 ± 3% immunostain positively for AQP1; conversely, 46 ± 4% of AQP1-expressing afferents co-express TRPV1 (Fig. 3G, H).

Developmental expression of AQP1 in DRG

To form a complete picture of not only the spatial but also the temporal expression of AQP1 in DRG, we next examined the developmental time course of its expression. We first detected AQP1 IR in the DRG of the mouse at E15.5 (Fig. 4A). Earlier embryos, such as the E14.5 embryo shown in Fig. 4B, did not contain detectable immunoreactivity for AQP1. Interestingly, E15.5 corresponds to the stage of mouse development at which the majority of nociceptors innervate the spinal cord.

Influence of tissue and nerve damage on AQP1 expression

We next looked for changes in the level of expression of AQP1 in the dorsal horn after peripheral stimuli known to alter the physiological properties of nociceptors, including CFA-induced persistent inflammation or sciatic axotomy. Three days after CFA injection into one hindpaw, we could detect no significant difference in the amount of AQP1 IR in the ipsilateral dorsal horn compared to the contralateral side (ipsilateral 16.9 ± 3.3 A.U. vs. contralateral 24.9 ± 2.7 A.U.; p=0.1300). However, one week after complete transection of the sciatic nerve, we found that the ipsilateral dorsal horn showed an increased amount of AQP1 in the medial part of the superficial dorsal horn, which is the terminal zone of sciatic nerve afferents (ipsilateral 33.8 ± 3.0 A.U. vs. contralateral 20.0 ± 2.0 A.U.; p=0.0194).

Functional analysis of AQP1 in nociception

In the studies described above, we have shown that (1) AQP1 IR is present in the spinal cord in laminae associated with nociceptive processing, (2) AQP1 is present on the membrane of DRG neurons neurochemically defined as nociceptors, (3) the onset of AQP1 expression in DRG corresponds temporally to the formation of functional synaptic contacts between nociceptors and their postsynaptic partners in the spinal cord, and (4) AQP1 labeling in the dorsal horn changes after sciatic nerve lesion, a manipulation that results in an altered pain state. For these reasons, we hypothesized that AQP1 could have a functional role in nociceptive processing. To test this hypothesis, we initiated an extensive electrophysiological and behavioral analysis of wildtype (WT) mice and mice in which the gene that encodes AQP1 was deleted.

Electrophysiological characterization of AQP1 null mutant mice

In 31 mice (17 mutant and 14 WT), we recorded a total of 41 wide dynamic range (WDR) neurons located at 534 ± 25 μm and 571 ± 10 μm from the surface of the lumbar spinal cord in WT and mutant mice respectively. The location of the recording sites did not differ significantly between genotypes. Neurons from WT animals had a spontaneous firing rate of 0.13 ± 0.11 Hz, similar to that observed in null mutant animals, 0.28 ± 0.15 Hz (Fig. 5E, ctrl).

We characterized the responses of deep dorsal horn neurons to thermal stimulation by positioning a thermal probe that could be heated to 40°, 45°, and 50° C at the center of the receptive fields of the neurons. WT and mutant mice responded equally to thermal stimulation at each of these temperatures

(Fig. 5A-C, ctrl). At none of the temperatures did peak firing differ between genotypes (Fig. 5D).

To assess whether there is differential ability of dorsal horn neurons to become sensitized between WT and AQP1 mutant mice, we applied mustard oil (MO) to the paw around the thermal probe and monitored changes in firing in response to the same temperatures. As expected, mustard oil induced a profound increase in the activity of the neurons. However, there was no difference between genotypes in MO-evoked activity (Fig 5E, 10'). The mustard oil-evoked activity returned to pre-MO levels within 40 minutes after MO in both genotypes (Fig. 5E). These data show that there are no deficits in the acute response to a noxious chemical stimulus of deep dorsal horn spinal cord WDR neurons of the AQP1 mutant mice.

Ten minutes after MO the responses elicited by 40° C stimulation were significantly higher than their respective controls for both WT and mutant mice. This increase went back to baseline values within 60 minutes (Fig. 5A). No significant differences were observed in the responsiveness of the neurons to 40° C stimulation after MO between genotypes, showing that MO is able to induce normal sensitization of deep dorsal horn WDR neurons in animals lacking the AQP1 channel. Similarly to our findings at 40° C, no significant differences were observed in the time course of the responses to 45° (Fig. 5B) and 50° C (Fig. 5C) after MO between WT and mutant mice.

Behavioral characterization of AQP1 null mutant mice

As described previously (Ma et al., 1998), AQP1 mutant mice do not differ from wildtypes in survival, gross physical appearance, or organ

morphology, although they have a severe impairment in their ability to concentrate urine. We compared wildtype and AQP1 mutant mice in several acute pain models, including the hindpaw radiant heat, hot plate, and tail flick tests of thermal nociception, the von Frey test of mechanical nociception, and the intraplantar capsaicin test of chemical nociception (Fig. 6A-E). In each of these modalities we found no differences between genotypes. Next, we examined the animals in tests of inflammatory or persistent pain. Again, we found no differences based on genotype in the formalin test (Fig. 6F), mechanical allodynia induced in the spared nerve injury model of neuropathic pain (Fig. 6G), or thermal or mechanical allodynia in the setting of CFA-induced inflammation (Fig. 6G and data not shown).

Because AQP1 might alter fluid transport in the setting of inflammation we also assayed for possible changes in the magnitude of injury-induced edema. However, we did not detect differences between wildtype and AQP1 mutant mice in magnitude of edema (paw thickness scored as percent of baseline) evoked by capsaicin (WT 118 ± 11.6% vs. mutant 125 ± 8.9%, p=0.61), formalin (WT 151 ± 18.0% vs. mutant 135 ± 13.4%, p=0.53), or CFA (WT 120-157% vs. mutant 132-154%, p=0.39). Finally, we observed no difference between WT and mutant animals in flinching behavior evoked by hypoosmotic challenge in the setting of PGE2-induced inflammation (Alessandri-Haber et al., 2003; WT 10.0 ± 4.0 flinches vs. mutant 11.4 ± 3.1 flinches, p=0.79).

Lastly, we tested the integrity of the neurogenic inflammatory response by applying mustard oil topically and measuring the amount of extravasated Evans Blue dye in the inflamed skin. AQP1 mutant mice appear to have normal extravasation responses, since they showed no difference from

wildtype mice in this assay (WT 0.103 ± 0.017 A.U. vs. mutant 0.147 ± 0.028 A.U., p=0.21).

Discussion

The present study provides the first comprehensive analysis of the expression of a member of the aquaporin family of water channels in primary sensory neurons. We found that a very large population of DRG neurons expresses mRNA and contains protein for AQP1, and that these neurons colabel for markers of presumed nociceptors, including TRPV1 and substance P. In fact, Patapoutian and colleagues (personal communication), in a microarray analysis that investigated differences between wildtype and trkA knockout mice (which lack all small diameter nociceptive DRG neurons), found that mRNA encoding for AQP1 is likely the most abundant species in C fiber neurons. We also demonstrate that AQP1 protein is trafficked to both the central and peripheral axon branches of the primary afferents, and that it is localized to the plasma membrane of axons and synaptic terminals in the superficial dorsal horn, where it presumably can function as a native water channel. On the other hand, although we found that sciatic nerve transection, a manipulation that produces changes in nociceptor physiology, alters the amount of AQP1 protein in primary afferent terminals, neither electrophysiological nor a very comprehensive behavioral analysis uncovered differences in nociceptive processing between mice lacking AQP1 and wildtype mice. Thus the functional significance of this water channel in sensory neurons remains a mystery.

In an earlier study, Solenov et al. (2002) showed AQP1 immunoreactivity in the superficial dorsal horn and provided some evidence that changes in thickness of spinal cord slices in response to hypoosmolar conditions may be mediated in part by AQP1. While that study established a method for mapping changes in thickness of nervous tissue in vitro, it did not address why what seems to be a rather generalized function, namely sensitivity to swelling in CNS tissue, would be localized only to the terminal region of nociceptors.

An alternative point of view suggested by Yool and colleagues is that AQP1 acts as a cyclic nucleotide-gated ion channel (Yool et al., 1996; Anthony et al., 2000). However, several other labs have failed to replicate this result (Agre et al., 1997; Sasaki et al., 1997; Verkman and Yang, 1997; Deen et al., 1997; Fischbarg et al., 1997; Patil et al., 1997), and we did not pursue the hypothesis further in our study.

Because most of the studies that have been done describing AQP1 expression during development have been performed in species other than mouse, it is difficult to directly compare time of onset of AQP1 protein expression in DRG with that in other tissues. Bondy et al. (1993) found that rat kidney and red blood cells do not contain detectable AQP1 protein until soon after birth, while choroid plexus expresses AQP1 from E15 (the earliest time point examined) through adulthood. It appears likely that AQP1 is expressed earlier in DRG than in kidney or red blood cells; however, caution should be taken when comparing studies using different methods in different, though related, species. Interestingly, at E15.5 in the mouse the majority of fine cutaneous afferents penetrate the superficial dorsal horn and make

synaptic contacts. However, because AQP1 null mutant mice do not have altered nociception, it is difficult to know if this temporal correspondence has a functional relevance.

The major question left unanswered by this study is, what is the contribution, if any, of AQP1 to nociceptive processing? Given its remarkably restricted expression it seems unlikely that it is acting purely as a "housekeeping gene". However, mice lacking the AQP1 gene have normal electrophysiological responses to acute thermal stimuli and sensitize normally after tissue injury produced by topical mustard oil. Additionally, they have normal behavioral responses to acute noxious thermal, mechanical, and chemical stimuli, and develop allodynia and hyperalgesia comparable to wildtype mice in models of persistent pain. Finally, and perhaps surprisingly given that the AQP1 gene encodes a water channel, we found that tissue injury-induced neurogenic and non-neurogenic inflammatory responses where edema is prominent were indistinguishable in wildtype and mutant mice.

Of course, as in all studies in which a gene is knocked out throughout the development and life of the animal, compensation by other molecules may occur. It is not known whether any other aquaporins are expressed in sensory neurons, nor what other molecules may be differentially regulated in the absence of AQP1. To fully exclude a possible involvement of AQP1 in nociceptive processing it will be necessary to create an acute, inducible mutation or to develop a specific blocker of this channel that can be delivered directly to the primary afferent neurons.

In conclusion, our studies demonstrate that despite the abundant and restricted expression of AQP1 in nociceptive primary afferent neurons, this

channel is not required for normal pain processing, and the physiological function of neuronal AQP1 remains unresolved.

References

Agre P, Lee MD, Devidas S, Guggino WB (1997) Aquaporins and ion conductance. Science 275:1490; author reply 1492.

Agre P, King LS, Yasui M, Guggino WB, Ottersen OP, Fujiyoshi Y, Engel A, Nielsen S (2002) Aquaporin water channels--from atomic structure to clinical medicine. J Physiol 542:3-16.

Alessandri-Haber N, Yeh JJ, Boyd AE, Parada CA, Chen X, Reichling DB, Levine JD (2003) Hypotonicity induces TRPV4-mediated nociception in rat. Neuron 39:497-511.

Anthony TL, Brooks HL, Boassa D, Leonov S, Yanochko GM, Regan JW, Yool AJ (2000) Cloned human aquaporin-1 is a cyclic GMP-gated ion channel. Mol Pharmacol 57:576-588.

Bondy C, Chin E, Smith BL, Preston GM, Agre P (1993) Developmental gene expression and tissue distribution of the CHIP28 water-channel protein. Proc Natl Acad Sci U S A 90:4500-4504.

Castle NA (2005) Aquaporins as targets for drug discovery. Drug Discov Today 10:485-493.

Chaplan SR, Bach FW, Pogrel JW, Chung JM, Yaksh TL (1994) Quantitative assessment of tactile allodynia in the rat paw. J Neurosci Methods 53:55-63.

Deen PM, Mulders SM, Kansen SM, van Os CH (1997) Aquaporins and ion conductance. Science 275:1491; author reply 1492.

Fischbarg J, Kuang K, Li J, Iserovich P, Wen Q (1997) Aquaporins and ion conductance. Science 275:1491-1492; author reply 1492.

Kim IB, Lee EJ, Oh SJ, Park CB, Pow DV, Chun MH (2002) Light and electron microscopic analysis of aquaporin 1-like-immunoreactive amacrine cells in the rat retina. J Comp Neurol 452:178-191.

Ma T, Yang B, Gillespie A, Carlson EJ, Epstein CJ, Verkman AS (1998) Severely impaired urinary concentrating ability in transgenic mice lacking aquaporin-1 water channels. J Biol Chem 273:4296-4299.

Nielsen S, Smith BL, Christensen EI, Agre P (1993) Distribution of the aquaporin CHIP in secretory and resorptive epithelia and capillary endothelia. Proc Natl Acad Sci U S A 90:7275-7279.

Patil RV, Han Z, Wax MB (1997) Aquaporins and ion conductance. Science 275:1492; author reply 1492.

Sasaki S, Uchida S, Kuwahara M, Fushimi K, Marumo F (1997) Aquaporins and ion conductance. Science 275:1490-1491; author reply 1492.

Shields SD, Eckert WA, 3rd, Basbaum AI (2003) Spared nerve injury model of neuropathic pain in the mouse: a behavioral and anatomic analysis. J Pain 4:465-470.

Snider WD, McMahon SB (1998) Tackling pain at the source: new ideas about nociceptors. Neuron 20:629-632.

Solenov EI, Vetrivel L, Oshio K, Manley GT, Verkman AS (2002) Optical measurement of swelling and water transport in spinal cord slices from aquaporin null mice. J Neurosci Methods 113:85-90.

Verkman AS, Yang B (1997) Aquaporins and ion conductance. Science 275:1491; author reply 1492.

Yool AJ, Stamer WD, Regan JW (1996) Forskolin stimulation of water and cation permeability in aquaporin 1 water channels. Science 273:1216-1218.

Zeitz KP, Guy N, Malmberg AB, Dirajlal S, Martin WJ, Sun L, Bonhaus DW, Stucky CL, Julius D, Basbaum AI (2002) The 5-HT3 subtype of serotonin receptor contributes to nociceptive processing via a novel subset of myelinated and unmyelinated nociceptors. J Neurosci 22:1010-1019.

Figure 1. AQP1 is expressed in primary sensory neurons. (A) Dense AQP1 immunoreactivity (IR) is present in laminae I and II of the lumbar dorsal horn, with some fibers arborizing ventrally. (B) Absence of AQP1 IR in an AQP1 -/- mouse spinal cord demonstrates antibody specificity. AQP1 IR (C) and mRNA (D) are present in a subset of neurons in DRG. (E) As neurons in the spinal cord do not express AQP1 mRNA, we conclude that immunoreactive signal in (A) derives solely from axon terminals of primary afferents. (F) Absence of signal after hybridization with a sense probe confirms specificity of the labeling with the antisense probe. (G) AQP1 immunoreactive axons and terminals in the bladder illustrate that peripheral terminals of primary afferents express the channel. Scale bars in A, B, D, F = 100 μm; C, G = 50 μm; E = 500 μm.

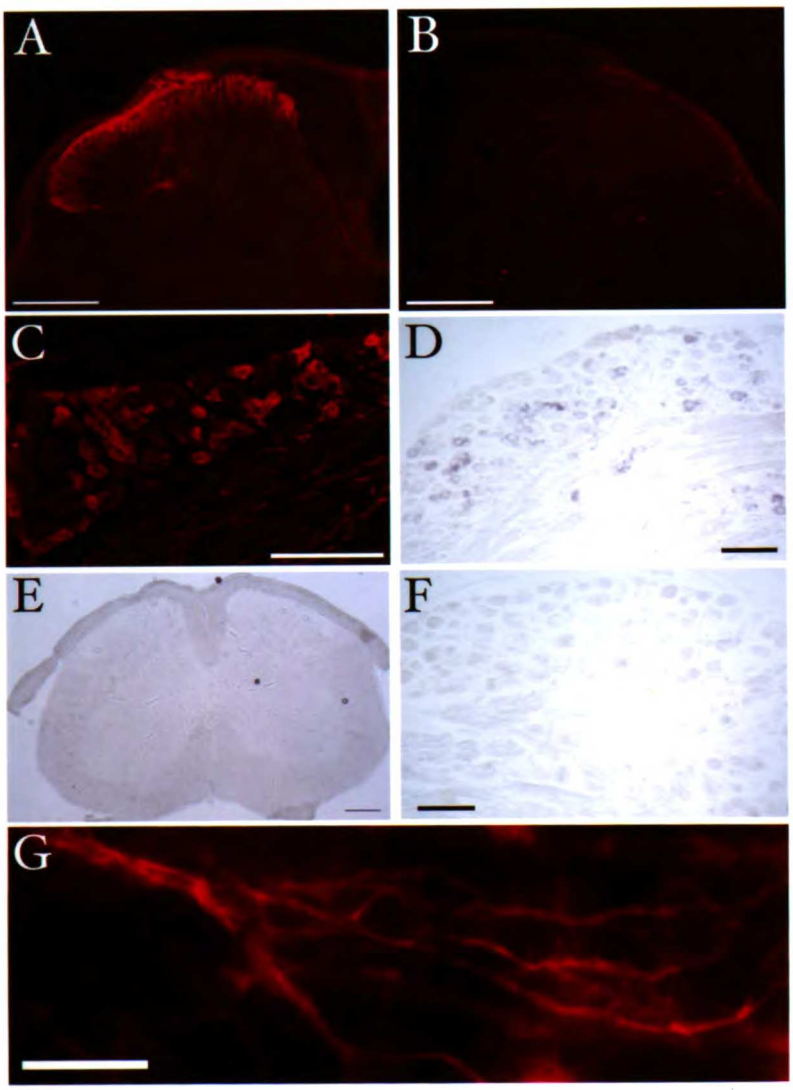
A
B
C
D
E
F
G

Figure 2. Ultrastructural localization of AQP1 IR in superficial dorsal horn. (A) The very dense AQP1-immunolabeling is largely restricted to the plasma membrane of unmyelinated axons, with (B) occasional labeling of myelinated fibers. (C) Synaptic terminal membrane, with the exception of the region at the synaptic density (arrow), is heavily labeled. Scale bars in all panels represent 1.0 μm.

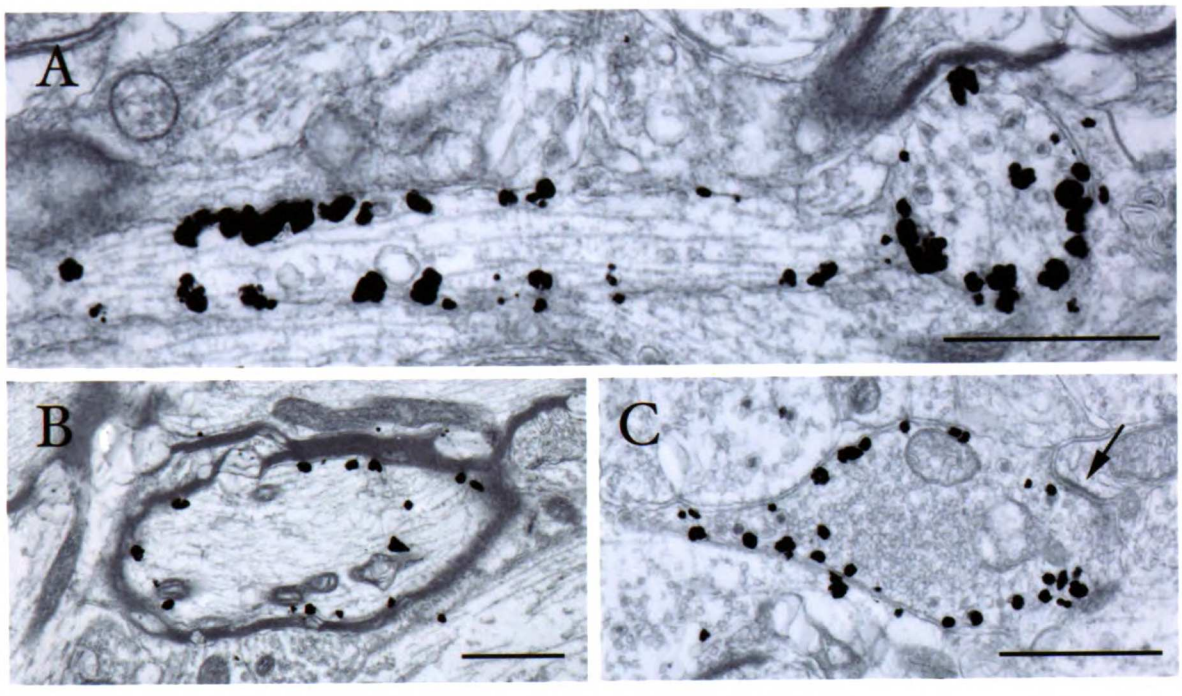
A
B
C

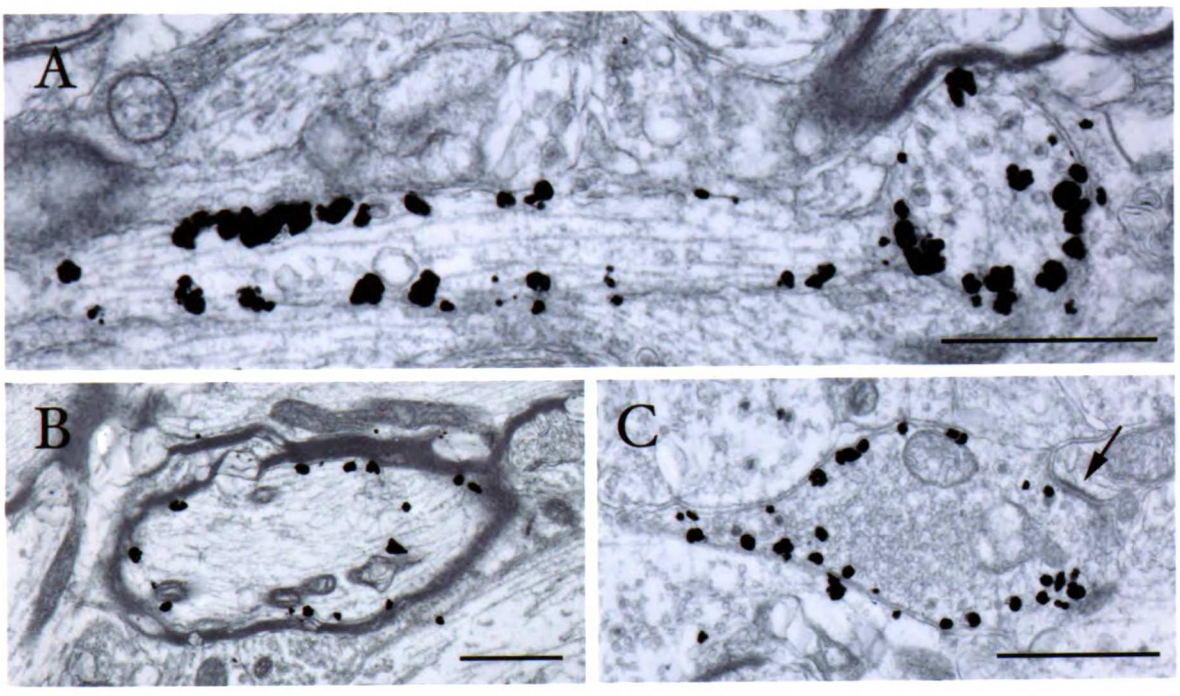
A
B
C

Figure 3. AQP1 IR colocalizes with markers of presumed nociceptors. AQP1 (A, C, E, G) does not overlap with neurofilament 200 (B), but is coexpressed with IB_4 (D), substance P (F), and TRPV1 (H). Arrows indicate double-labeled cells; arrowheads indicate single-labeled cells. Scale bar in F applies to A-F; scale bar in H applies to G-H. Scale bars represent 100 μm.

Figure 4. Developmental onset of expression of AQP1 IR in DRG. Immunoreactivity for AQP1 is not detectable in mouse DRG at E14.5 (A), but is present at E15.5 (B). In both panels, the central canal of the spinal cord is on the left and the DRG is at the lower right. Scale bar = 10 μm.

A
B

Figure 5. Electrophysiological characterization of AQP1 -/- mice. (A-C) Mean firing rates of deep dorsal horn WDR neurons in response to 40° (A), 45° (B), and 50° C (C) stimuli applied to their receptive fields, prior to (ctrl) and 10, 40, and 60 minutes after the administration of mustard oil. (D) Peak response of the neurons to the three temperatures prior to the administration of MO. (E) Basal activity of the neurons before and after mustard oil.

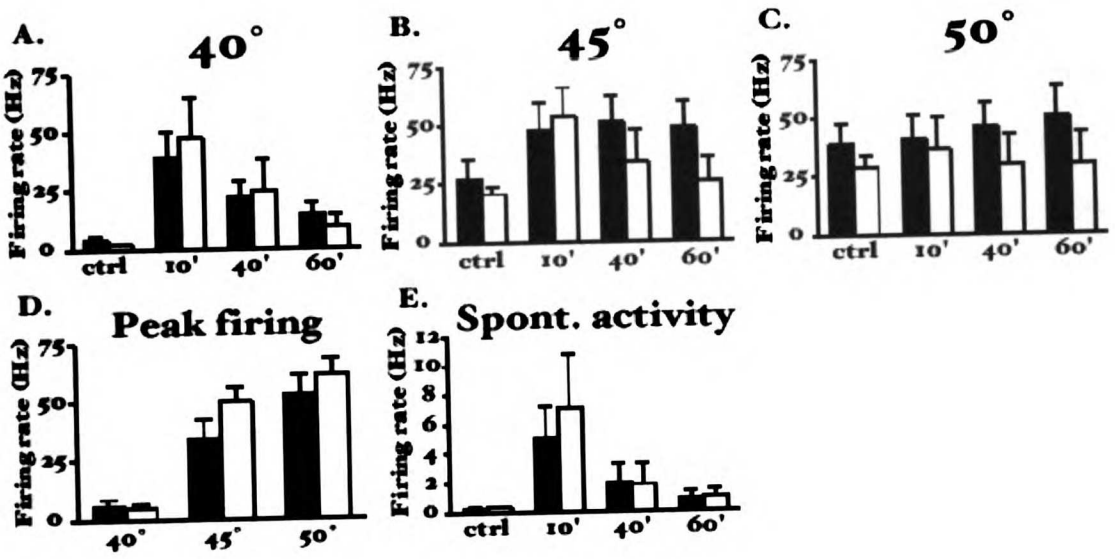
A.
40°
B.
45°
C.
50°
Firing rate (Hz)
75
50
25
0
ctrl
10'
40'
60'
D.
Peak firing
40°
45°
50°
E.
Spont. activity
12
10
8
6
4
2

Figure 6. Behavioral characterization of AQP1 -/- mice. Wildtype (black bars, ■) and AQP1 -/- mice (white bars, ○) did not differ in their behavioral responses in a battery of acute and persistent pain tests, including (A) hindpaw radiant heat, (B) hot plate at 50.0° C, 52.5° C, or 55.0° C, (C) tail flick tested during the morning or the afternoon, (D) von Frey test using the up-down method, (E) licking response after intraplantar injection of capsaicin, (F) formalin test, (G) mechanical allodynia induced in the spared nerve injury model of neuropathic pain, or (H) thermal allodynia induced by intraplantar CFA injection.

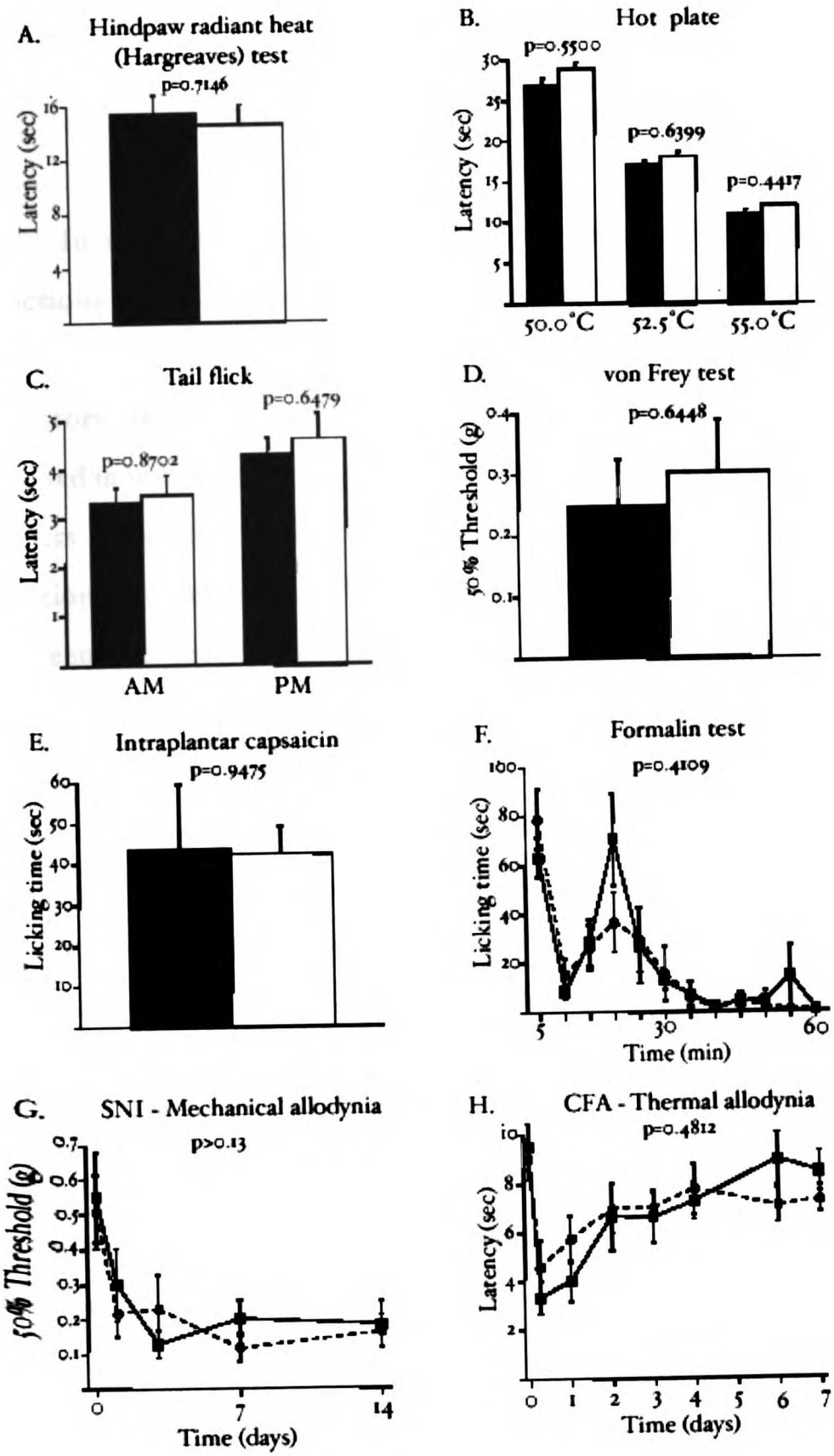
A.
Hindpaw radiant heat (Hargreaves) test
p=0.7146
Latency (sec)
B.
Hot plate
p=0.5500
p=0.6399
p=0.4417
Latency (sec)
50.0°C
52.5°C
55.0°C
C.
Tail flick
p=0.8702
p=0.6479
Latency (sec)
AM
PM
D.
von Frey test
p=0.6448
50% Threshold (g)
E.
Intraplantar capsaicin
p=0.9475
Licking time (sec)
F.
Formalin test
p=0.4109
Licking time (sec)
Time (min)
G.
SNI - Mechanical allodynia
p>0.13
50% Threshold (g)
Time (days)
H.
CFA - Thermal allodynia
p=0.4812
Latency (sec)
Time (days)

Chapter 4

The mammalian olfactory system

In mammals, the sense of smell is important for a variety of vital functions including reproductive and social behaviors, neuroendocrine regulation, foraging and determination of food quality, recognition of predators, and emotional responses. Detailed delineation of the circuitry involved in transmitting olfactory information from the environment to neural centers where it is processed is necessary for understanding how these functions are accomplished. Much progress has been made in this field between the description by classical histologists of the cell types and lamination that are characteristic of the olfactory bulb and recent advances such as the discovery of the molecular nature of odorant receptors and functional imaging studies showing this neural transduction system in action (Ramon y Cajal, 1890, cited in Pinching and Powell, 1971a; Buck and Axel, 1991; Rubin and Katz, 1999). Because the final part of my dissertation deals with AQP1 expression in the olfactory bulb, I present here a review of current knowledge about the architecture and function of the olfactory sensory system.

A century ago, Ramon y Cajal and his contemporaries first described the orderly lamination of the olfactory bulb. On the superficial surface of the olfactory bulb lies the olfactory nerve layer, composed of the axons of olfactory receptor neurons (ORNs) and their associated glial cells, the olfactory ensheathing glia (OEGs). Slightly deeper is the glomerular layer,

made up of the distinctive spherical or ovoid structures known as glomeruli inside of which the termini of ORNs communicate with the dendrites of neurons that project to other parts of the brain. The glomeruli are encircled by the somata of periglomerular (PG) cells. These interneurons also take part in the glomerular interaction between olfactory afferents and output neurons. The next layer, the external plexiform layer, has a relatively low cell density but contains many dendrites of mitral, tufted, and granule cells as well as the somata of some tufted cells. Immediately subjacent to the external plexiform layer is the mitral cell layer, a tight, thin band of cell bodies of the principal output neurons of the olfactory bulb, whose morphology reminded Ramon y Cajal of a bishop's miter. In the heart of the olfactory bulb is the granule cell layer, which contains the GABAergic granule cells that serve to modulate mitral and tufted cells via dendrodendritic synapses in the external plexiform layer (Shipley et al., 1995; Purves et al., 2001). More detail on each of the steps in the transmission of olfactory sensory information is given below.

When a volatile odorant enters the nasal cavity, it encounters the main olfactory epithelium (MOE), a thin sheet of tissue located at the top of the nasal passage, lining the labyrinthine convolutions of bone known as the turbinates. The MOE is a pseudostratified epithelium composed of ORNs, sustentacular or supporting cells, basal cells, and mucus-secreting glands situated on a lamina propria (Shipley et al., 1995; Purves et al., 2001). ORNs are bipolar: a single dendrite reaches toward the periphery while a single unmyelinated axon penetrates the basal lamina and joins other ORN axons to eventually form the first cranial nerve. The dendrites of ORNs have a highly specialized morphology to facilitate reception of odors, forming cilia that

extend into the mucus layer that covers the epithelium. The superficial location of the ORNs allows for direct access to odorant molecules, but also exposes them to possible damage from pollutants, microorganisms, and dangerous chemicals in the environment. To maintain the integrity of the olfactory sensory apparatus, continual regeneration of ORNs occurs throughout the life of the animal, with an estimated turnover rate of 6-8 weeks in rodents (Graziadei and Graziadei, 1979). The basal cells act as stem cells, dividing to become new ORNs. This is one of the few examples of neural regeneration in mature animals and can be used as a model system to study renewal of neural tissue and reestablishment of functional connections after injury or disease.

The cilia of the ORNs appear to be the site of sensory signal transduction based on electrophysiological studies of dissociated ORNs in which odorants applied selectively to the cilia, but not to the cell soma, evoked a robust response (Firestein et al., 1990). The elusive identity of the odorant receptor molecules frustrated research on signal transduction and coding of olfactory stimuli until 1991 when Buck and Axel reported their discovery that a novel family of G-protein coupled receptors was responsible for recognizing such signals. Each odorant receptor recognizes one or a few structurally similar odorants, and each ORN expresses only one of the estimated 1000 different odorant receptor genes in the mouse (there are about 100-200 in humans). Consequently, each ORN is sensitive to a small set of chemical stimuli that define a tuning curve (Purves et al., 2001).

What are the intracellular events that occur between binding of an odorant to its receptor and transmission of a neural signal to the olfactory

bulb? First, a conformation change in the odorant receptor causes activation of an olfactory-specific G-protein, $G\alpha_{olf}$ (Jones and Reed, 1989). This then leads to increased production of cyclic AMP by adenylyl cyclase and of inositol 1,4,5-triphosphate by phospholipase C (Jones and Reed, 1989; Schandar et al., 1998; Takeuchi and Kurahashi, 2003). These second messengers in turn cause opening of cation channels, eventually resulting in depolarization of the neuron, action potential generation, and neurotransmitter release.

From the main olfactory epithelium, odorant-related information travels in the olfactory nerve as it passes through the cribriform plate of the ethmoid bone to the olfactory bulb. This first cranial nerve is composed not only of the axons of ORNs but also olfactory ensheathing glial cell bodies and processes. The OEGs are small, multipolar cells whose long processes envelop the axons of ORNs, but due to the absence of myelin-like markers (e.g. myelin basic protein, galactocerebroside) and to their ultrastructural morphology they are not thought to myelinate these axons (Devon and Doucette, 1992; Franklin et al., 1996; Imaizumi et al., 2000). OEGs appear to represent a chemically unique type of glia with features intermediate between astrocytes and Schwann cells, although they derive from a distinct ontological origin from each of these types. Thus, they express $p75^{NTR}$ and Po like Schwann cells, as well as low levels of GFAP, an astrocyte marker (Wewetzer et al., 2002). Some heterogeneity exists within the population of OEGs and some authors have preferred to subclassify them as either Schwann cell-like or astrocyte-like (Pixley, 1992), or with respect to their sublaminar organization within the olfactory nerve layer and expression of neuropeptides (Au et al., 2002).

ORNs are one of the few neuronal types to span the boundary between peripheral and central nervous system, and are also one of the few types of neurons to regenerate continuously throughout the life of the organism. Because of their unique association with ORNs, OEGs have been hypothesized to contribute to this capacity to regrow and reform functional connections. Therefore, much recent interest has focused on the application of OEGs to spinal cord injury models, with some success in encouraging long distance regrowth of injured axons and functional recovery (Ramon-Cueto et al., 2000; Lopez-Vales et al., 2005; Li et al., 1997).

Upon entering the olfactory bulb, the ORN axons expressing a particular odorant receptor converge upon a small number (usually two) of bilaterally symmetrical glomeruli in the olfactory bulbs whose position is relatively invariant across individuals (Mombaerts et al., 1996). Glomeruli are areas of cell-poor neuropil approximately 50-120 μm in diameter that serve as hubs of synaptic communication between ORN axons and dendrites of second order neurons, the mitral and tufted cells (Pinching and Powell, 1971b). Periglomerular cells form a shell around each one and extend axons into and between glomeruli, receiving inputs from ORNs and making reciprocal synapses with mitral cells; they are thus well positioned to modulate the flow of synaptic information at this junction. While the exact nature of this modulation is unknown, it has been observed that manipulations to olfactory epithelium have indirect consequences on protein levels in PG neurons (Stone et al., 1991; Baker et al., 1983, 1988).

Continual turnover of ORNs in the main olfactory epithelium implies continual degradation and reformation of synapses between these afferents

and their postsynaptic partners in the olfactory bulb, but it has been discovered that there is constant renewal of interneurons in the olfactory bulb itself as well. In particular, newly generated PG and granule cells migrate from the subventricular zone through the rostral migratory stream and integrate into the existing circuitry of their respective layers, forming functional synaptic contacts there (Lois and Alvarez-Buylla, 1994; Belluzzi et al., 2003). When first reported, this discovery challenged the dogma that the brain cannot generate new neurons beyond the developmental period. However, it has now been accepted as fact and forms the basis for many studies on the therapeutic potential of adult neurogenesis in neurological disorders and aging (Hoglinger et al., 2004; Jin et al., 2003; Malberg et al., 2000; Zhang et al., 2001).

The projection neurons of the olfactory bulb are the mitral and tufted cells. Although many authors have traditionally segregated mitral and tufted cells into separate categories on the basis of the location of their cell bodies, their common inputs, central projections, and ultrastructurally defined synaptic characteristics argue that they in fact form a single class (Pinching and Powell, 1971c). Mitral/tufted cells have one apical dendrite that enters a single glomerulus and branches extensively, forming a tuft-like arborization (Pinching and Powell, 1971b). Each glomerulus has been estimated to contain the dendrites of around 25 mitral/tufted cells and up to 25,000 ORN axons (Purves et al., 2001). Such convergence likely serves to ensure transmission of real odor signals and eliminate spurious signaling by uncorrelated noise in the system. In addition to receiving inputs at the apical dendrite from ORNs and PG cells, mitral/tufted cells also form lateral dendrites onto which

dendrodendritic synapses are made with granule cells (Shipley et al., 1995). Once again, little is known about the interaction between mitral/tufted cells and granule cells, but it is assumed that their interaction is important for local lateral inhibition in the olfactory bulb.

Upon leaving the olfactory bulb via the lateral olfactory tract, axons of mitral/tufted cells innervate a group of structures collectively referred to as primary olfactory cortex, including the anterior olfactory nucleus, indusium grisium, infralimbic cortex, olfactory tubercle, piriform cortex, periamygdaloid cortex, and entorhinal cortex (de Olmos et al., 1978; Shipley and Adamek, 1984; Haberly and Price, 1977). The olfactory system is unique among sensory systems for making direct connections with cortical areas without first going through the thalamus. The various regions of the primary olfactory cortex then project to a wide range of higher order structures involved in such functions as autonomic adjustments (hypothalamus and medial frontal cortex); integration of olfactory, gustatory, and visceral sensation (insular and orbital cortices); memory (hippocampus); and emotion (amygdala and ventral striatum) (Newman and Winans, 1980; Shipley and Geinisman, 1984; Schwerdtfeger et al., 1990).

In conclusion, while much has been described concerning the anatomy and function of the olfactory sensory system, it is also clear that much more remains to be discovered. In the final chapter of this dissertation, I present evidence for the expression of AQP1 protein in what appears to be a previously undescribed and uncharacterized fiber tract within the olfactory bulb.

References

Au WW, Treloar HB, Greer CA (2002) Sublaminar organization of the mouse olfactory bulb nerve layer. J Comp Neurol 446:68-80.

Baker H, Towle AC, Margolis FL (1988) Differential afferent regulation of dopaminergic and GABAergic neurons in the mouse main olfactory bulb. Brain Res 450:69-80.

Baker H, Kawano T, Margolis FL, Joh TH (1983) Transneuronal regulation of tyrosine hydroxylase expression in olfactory bulb of mouse and rat. J Neurosci 3:69-78.

Belluzzi O, Benedusi M, Ackman J, LoTurco JJ (2003) Electrophysiological differentiation of new neurons in the olfactory bulb. J Neurosci 23:10411-10418.

Buck L, Axel R (1991) A novel multigene family may encode odorant receptors: a molecular basis for odor recognition. Cell 65:175-187.

de Olmos J, Hardy H, Heimer L (1978) The afferent connections of the main and the accessory olfactory bulb formations in the rat: an experimental HRP-study. J Comp Neurol 181:213-244.

Devon R, Doucette R (1992) Olfactory ensheathing cells myelinate dorsal root ganglion neurites. Brain Res 589:175-179.

Firestein S, Shepherd GM, Werblin FS (1990) Time course of the membrane current underlying sensory transduction in salamander olfactory receptor neurones. J Physiol 430:135-158.

Franklin RJ, Gilson JM, Franceschini IA, Barnett SC (1996) Schwann cell-like myelination following transplantation of an olfactory bulb-ensheathing cell line into areas of demyelination in the adult CNS. Glia 17:217-224.

Graziadei PP, Graziadei GA (1979) Neurogenesis and neuron regeneration in the olfactory system of mammals. I. Morphological aspects of differentiation and structural organization of the olfactory sensory neurons. J Neurocytol 8:1-18.

Haberly LB, Price JL (1977) The axonal projection patterns of the mitral and tufted cells of the olfactory bulb in the rat. Brain Res 129:152-157.

Hoglinger GU, Rizk P, Muriel MP, Duyckaerts C, Oertel WH, Caille I, Hirsch EC (2004) Dopamine depletion impairs precursor cell proliferation in Parkinson disease. Nat Neurosci 7:726-735.

Imaizumi T, Lankford KL, Kocsis JD (2000) Transplantation of olfactory ensheathing cells or Schwann cells restores rapid and secure conduction across the transected spinal cord. Brain Res 854:70-78.

Jin K, Sun Y, Xie L, Batteur S, Mao XO, Smelick C, Logvinova A, Greenberg DA (2003) Neurogenesis and aging: FGF-2 and HB-EGF restore neurogenesis in hippocampus and subventricular zone of aged mice. Aging Cell 2:175-183.

Jones DT, Reed RR (1989) Golf: an olfactory neuron specific-G protein involved in odorant signal transduction. Science 244:790-795.

Li Y, Field PM, Raisman G (1997) Repair of adult rat corticospinal tract by transplants of olfactory ensheathing cells. Science 277:2000-2002.

Lois C, Alvarez-Buylla A (1994) Long-distance neuronal migration in the adult mammalian brain. Science 264:1145-1148.

Lopez-Vales R, Fores J, Verdu E, Navarro X (2005) Acute and delayed transplantation of olfactory ensheathing cells promote partial recovery after complete transection of the spinal cord. Neurobiol Dis.

Malberg JE, Eisch AJ, Nestler EJ, Duman RS (2000) Chronic antidepressant treatment increases neurogenesis in adult rat hippocampus. J Neurosci 20:9104-9110.

Mombaerts P, Wang F, Dulac C, Chao SK, Nemes A, Mendelsohn M, Edmondson J, Axel R (1996) Visualizing an olfactory sensory map. Cell 87:675-686.

Newman R, Winans SS (1980) An experimental study of the ventral striatum of the golden hamster. II. Neuronal connections of the olfactory tubercle. J Comp Neurol 191:193-212.

Pinching AJ, Powell TP (1971a) The neuropil of the periglomerular region of the olfactory bulb. J Cell Sci 9:379-409.

Pinching AJ, Powell TP (1971b) The neuropil of the glomeruli of the olfactory bulb. J Cell Sci 9:347-377.

Pinching AJ, Powell TP (1971c) The neuron types of the glomerular layer of the olfactory bulb. J Cell Sci 9:305-345.

Pixley SK (1992) The olfactory nerve contains two populations of glia, identified both in vivo and in vitro. Glia 5:269-284.

Purves D, Augustine GJ, Fizpatrick D, Katz LC, LaMantia A-S, McNamara JO, Williams SM, eds (2001) Neuroscience, Second Edition. Sunderland, MA: Sinauer.

Ramon-Cueto A, Cordero MI, Santos-Benito FF, Avila J (2000) Functional recovery of paraplegic rats and motor axon regeneration in their spinal cords by olfactory ensheathing glia. Neuron 25:425-435.

Rubin BD, Katz LC (1999) Optical imaging of odorant representations in the mammalian olfactory bulb. Neuron 23:499-511.

Schwerdtfeger WK, Buhl EH, Germroth P (1990) Disynaptic olfactory input to the hippocampus mediated by stellate cells in the entorhinal cortex. J Comp Neurol 292:163-177.

Shipley MT, Adamek GD (1984) The connections of the mouse olfactory bulb: a study using orthograde and retrograde transport of wheat germ agglutinin conjugated to horseradish peroxidase. Brain Res Bull 12:669-688.

Shipley MT, Geinisman Y (1984) Anatomical evidence for convergence of olfactory, gustatory, and visceral afferent pathways in mouse cerebral cortex. Brain Res Bull 12:221-226.

Shipley MT, McLean JH, Ennis M (1995) Olfactory system. In: The rat nervous system, Second Edition (Paxinos G, ed), pp 899-926. San Diego: Academic Press.

Stone DM, Grillo M, Margolis FL, Joh TH, Baker H (1991) Differential effect of functional olfactory bulb deafferentation on tyrosine hydroxylase and glutamic acid decarboxylase messenger RNA levels in rodent juxtaglomerular neurons. J Comp Neurol 311:223-233.

Takeuchi H, Kurahashi T (2003) Identification of second messenger mediating signal transduction in the olfactory receptor cell. J Gen Physiol 122:557-567.

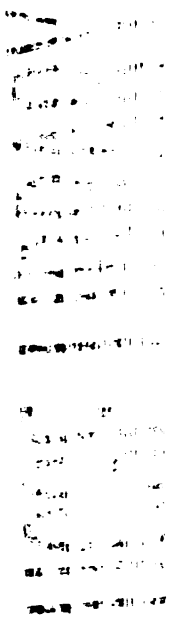

Wewetzer K, Verdu E, Angelov DN, Navarro X (2002) Olfactory ensheathing glia and Schwann cells: two of a kind? Cell Tissue Res 309:337-345.

Zhang R, Zhang L, Zhang Z, Wang Y, Lu M, Lapointe M, Chopp M (2001) A nitric oxide donor induces neurogenesis and reduces functional deficits after stroke in rats. Ann Neurol 50:602-611.

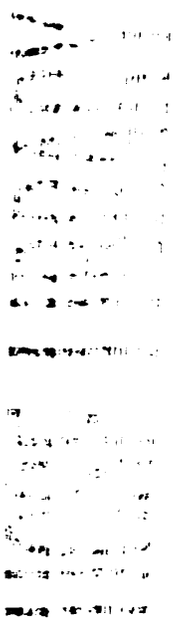

Chapter 5

Immunohistochemical localization of aquaporin 1 in the mouse olfactory bulb

Shannon D. Shields and Allan I. Basbaum

Depts. of Anatomy and Physiology and W. M. Keck Foundation Center for Integrative Neuroscience, University of California at San Francisco

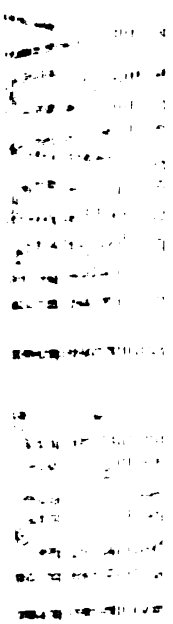

Abstract

We present here the first evidence for expression of a member of the aquaporin family of water channels in the mammalian olfactory system. AQP1 immunoreactivity (IR) is present in a dense meshwork of fine fibers that cover the superficial surface of the olfactory bulb and make numerous branches into the glomerular layer, sometimes seeming to wrap around individual glomeruli. We present evidence that this labeling does not derive from olfactory receptor neurons, olfactory ensheathing glia, astrocytes, periglomerular cells, or trigeminal axons. Instead, we propose that AQP1 may be a marker of a unique, previously unrecognized fiber tract at the interface of the olfactory nerve layer and the glomerular layer of the mouse olfactory bulb.

Introduction

In mammals, the sense of smell is essential for a variety of critical functions including reproductive and social behaviors, neuroendocrine regulation, foraging and determination of food quality, recognition of predators, and emotional responses. Detailed delineation of the circuitry involved in transmitting olfactory information from the environment to neural centers where it is processed is necessary for understanding how these functions are accomplished. Much progress has been made in this field since the description by classical histologists of the cell types and lamination that are characteristic of the olfactory bulb (Ramon y Cajal, 1890, cited in Pinching and Powell, 1971a). Of particular note are the elucidation of the molecular nature of odorant receptors (Buck and Axel, 1991) and functional imaging studies showing this neural transduction system in action (Rubin and Katz, 1999).

The aquaporins (AQPs) comprise an ancient family of integral membrane proteins that function as water-selective channels in animals, plants, and microorganisms. To date, thirteen mammalian aquaporins have been identified (for review, see Castle, 2005). AQP1, the archetypal member of this family, is a constitutively open, bidirectional water channel expressed in red blood cells, renal proximal tubules, capillary endothelium, choroid plexus, and other tissues where water permeability is important to function (Agre et al., 2002). Recently, we have also described the expression of AQP1 in primary somatosensory neurons of the mouse (Shields et al., 2006).

In the course of our earlier work characterizing the nervous system expression of AQP1 we discovered that this protein is also present in the

olfactory bulb. In this report we detail the expression of AQP1 in a fiber tract at the interface of the olfactory nerve layer and glomerular layer, and by extensive colocalization experiments demonstrate that olfactory bulb AQP1 protein does not derive from olfactory receptor neurons, olfactory ensheathing glia, periglomerular cells, astrocytes, or trigeminal axons. Instead, we propose that AQP1 may be a marker of a unique, previously unrecognized fiber tract in the mouse olfactory bulb.

Materials and Methods

All animal experiments were approved by the Institutional Animal Care and Use Committee of the University of California at San Francisco and were conducted in accordance with the National Institutes of Health Guide for the Care and Use of Laboratory Animals. AQP1 -/- mice (Ma et al., 1998) were originally provided by Drs. Alan Verkman and Geoffrey Manley (University of California, San Francisco) and were subsequently produced by interbreeding heterozygotes.

Tissue preparation. Adult mice (20-30 g) were deeply anesthetized with 100 mg/kg sodium pentobarbital and perfused transcardially with 0.1M phosphate-buffered saline (PBS) followed by 10% formalin in PBS. Brains and/or snouts were collected, post-fixed in the same fixative for 4 hours, and cryoprotected overnight in 30% sucrose in 0.1M PBS. Snouts were decalcified overnight in 250 mM EDTA and 50 mM phosphate buffer. Mice with Dlx1/Dlx2 and Dlx5 mutations die soon after birth, so tissue was collected from these lines at E18.5 or P0. These brains were immersion fixed in phosphate-buffered 4% paraformaldehyde, cryoprotected, embedded in OCT medium (Sakura

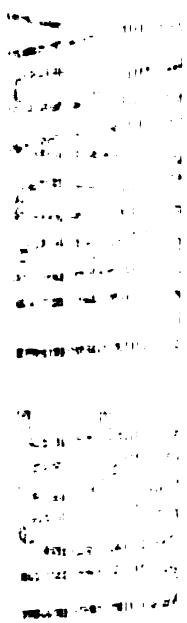

Finetech USA, Torrance, CA), and frozen before cutting. Brains from S100B-GFP mice (see Zou et al., 2004) were a generous gift from Dr. W. Thompson (University of Texas at Austin). Tissue was sectioned either on a freezing microtome at 30-40 µm and processed as free-floating sections or cut at 20-25 µm on a cryostat and processed on slides.

Immunohistochemistry. Immunohistochemical experiments were performed as described in Shields et al., 2006. Primary antisera were as follows: rabbit anti-AQP1 (1:10,000; Chemicon Inc., Temecula, CA), goat anti-OMP (1:7500; WAKO Chemicals USA, Richmond, VA), rabbit anti-$p75^{NTR}$ (1:2000; polyclonal antibody 9651, see Huber and Chao, 1995), rabbit anti-GFAP (1:2000; DAKO Cytomation California, Carpinteria, CA), monoclonal anti-NeuN (1:1000; Chemicon), monoclonal anti-TH (1:5000; RBI, Natick, MA). Secondary antisera were as follows: biotinylated goat anti-rabbit IgG (1:200; Vector, Burlingame, CA), Alexa 546 or 488 conjugated goat anti-rabbit, goat anti-mouse, donkey anti-rabbit, or donkey anti-goat IgG (all used at 1:700; all from Molecular Probes, Eugene, OR). Digital images were captured using a CCD camera attached to either a Nikon Eclipse or a Zeiss Axioscop 2 microscope.

In situ hybridization. Digoxygenin-labeled probes were transcribed from linearized pBluescript II SK vector (Stratagene, La Jolla, CA) containing a portion of the 3' untranslated region of the AQP1 cDNA (Shields et al., 2006). Hybridization was conducted as described previously (Zeitz et al., 2002). The hybridized probe was visualized by incubation with alkaline phosphatase-linked anti-digoxygenin Fab fragments (Roche, Mannheim, Germany) followed by reaction with 4-nitro blue tetrazolium chloride and 5-bromo-4-

chloro-3-indolylphosphate (Roche) according to the specifications of the manufacturer.

Results

Our initial observation of AQP1-like immunoreactivity (IR) was made in sagittal sections through the whole mouse brain. In this view (Fig. 1A), positive IR for AQP1 is readily apparent in the trigeminal nucleus caudalis (the medullary homologue of the spinal cord dorsal horn; see Shields et al., 2006), the choroid plexus (where it has previously been described by Nielsen et al., 1993), and the outer surface of the main olfactory bulb. We did not observe staining in the accessory olfactory bulb. There is no immunoreactivity in the brains of mice with a deletion of the AQP1 gene (data not shown). Examination at higher magnification of coronal sections through the bulb reveals that the AQP1 IR is present in the form of a dense meshwork of fine fibers that surround the entire bulb at its outer surface. These fibers make numerous branches into the glomerular layer, sometimes seeming to wrap around individual glomeruli (Fig 1B-D). Despite this dense fibrous network, we never observed unequivocal cell body labeling.

To determine the source of AQP1 in the olfactory bulb, we next performed a detailed examination of the various neuronal and glial elements that comprise the bulb. We first investigated olfactory receptor neurons (ORNs), the sensory afferents that transmit neural signals about olfactory stimuli to the brain. Like AQP1 IR, immunoreactivity for the ORN marker olfactory marker protein (OMP) is present in a dense band of fibers at the external surface of the bulb (Margolis and Tarnoff, 1973; Monti Graziadei et

al., 1977). However, in contrast to the OMP positive fibers, which terminate exclusively within the sharply defined borders of glomeruli, AQP1 positive fibers course between glomeruli, in a pattern clearly distinct from that of OMP (Fig. 2A-C). Consistent with this result, we did not observe AQP1 protein or mRNA in the main olfactory epithelium (MOE), using either immunohistochemistry or in situ hybridization (Fig. 2D, E). As this negative evidence may reflect low sensitivity for detection of AQP1 in the MOE, we also analyzed tissue from Dlx5 mutant mice, in which very few ORNs are born and even those that do develop never successfully innervate the olfactory bulb (Long et al., 2003). Figure 2H-K illustrates that AQP1 IR is completely normal in these mice, when compared to wildtype or heterozygous littermates. We conclude on the basis of these assays that AQP1 is not expressed in ORNs.

We next considered olfactory ensheathing glia (OEGs), a unique glial subtype that spans the PNS/CNS boundary enveloping olfactory afferents. Dissociated OEGs in culture, while retaining IR for $p75^{NTR}$, were completely lacking AQP1 IR (Fig. 2F, G). The calcium binding protein subunit S100B is another marker of olfactory ensheathing glia (Au et al., 2002; Astic et al., 1998). We acquired olfactory bulbs from mice expressing GFP under the control of the S100B promoter (Zuo et al., 2004) and used immunohistochemical techniques to assess colocalization between AQP1 IR and S100B-GFP (data not shown). While S100B positive cells are distributed throughout the full extent of the olfactory nerve layer, AQP1 IR is confined to the innermost part of this layer, adjacent to the glomerular layer. A few S100B positive profiles appear in deeper laminae where AQP1 IR is absent; these likely represent labeling in a subpopulation of astrocytes (Matus and Mughal,

1975; Chao et al., 1997). In all layers where it is observed, S100B staining is present in small foci of intense staining. Au et al (2002) suggested that these are glial cell bodies. This pattern differs considerably from that of AQP1 IR, which is present in elongated fibers that course within the olfactory nerve layer and occasionally enter the glomerular layer. These distinct staining patterns suggest different cellular origins of AQP1 and S100B. The final argument against olfactory ensheathing glia as the origin of the AQP1 IR comes again from our examination of olfactory bulbs from Dlx5 null mutant mice. In addition to lacking olfactory bulb innervation by ORNs, these mice are also devoid of OEGs (Long et al., 2003). As shown in Fig. 2I-L, AQP1 IR is intact in Dlx5 mutant mice that lack OEGs.

Next we investigated the possibility that astrocytes in the olfactory bulb are the source of AQP1 IR. As described previously (Bailey and Shipley, 1993), GFAP positive astrocytes are located in all layers of the olfactory bulb, but they are most densely concentrated in the glomerular layer. Because our AQP1 and GFAP antibodies were both raised in rabbit, we could not do a direct colocalization experiment and we were instead obligated to use different sections to determine the degree of overlap between the two markers. Figure 3 shows that the patterns of staining produced by the two markers are clearly distinct. Specifically, although AQP1 is located in long, fine fibers at the superficial edge of the glomerular layer and in the olfactory nerve layer, GFAP immunoreactivity is concentrated in the relatively short processes of stellate shaped cells located deeper in the bulb. These distinct staining patterns indicate that AQP1 IR does not derive from olfactory bulb astrocytes.

Periglomerular (PG) cells are a type of local circuit interneuron with small cell bodies that surround the glomeruli. They are known to interact with axons of ORNs as well as with dendrites of mitral/tufted cells (Kosaka et al., 1998). To determine whether PG cells could be the source of the AQP1 IR in the olfactory bulb, we performed double immunohistochemical studies using NeuN (a pan-neuronal marker) and tyrosine hydroxylase (TH), which is synthesized by PG cells (Mullen et al., 1992; Halasz et al., 1977). Neither marker colabeled with AQP1 IR (Fig. 4A-F). We next analyzed tissue from Dlx1/Dlx2 double mutant mice. These mice have a very specific developmental deficit of the olfactory bulb: despite having a normal laminar organization of the bulb, normal axonal projections from the bulb to other regions, and an intact olfactory topographic map, the periglomerular and granule cells of these mice never develop (Anderson et al., 1997; Bulfone et al., 1998). As illustrated in Figs. 4G-J, we found AQP1 IR to be intact in Dlx1/Dlx2 mutant mice when compared to their wildtype littermates (Fig. 4G-J). We conclude that AQP1 is not expressed in PG cells.

Finally, because AQP1 is expressed in sensory neurons of the trigeminal ganglion (Shields et al., 2006), and because some trigeminal afferents penetrate into the glomerular layer of the olfactory bulb (Shaefer et al., 2002), we next asked whether the dense AQP1 labeling derives from sensory afferents. To this end we performed double label immunohistochemistry using another generalized marker for small diameter trigeminal axons, calcitonin gene related peptide (CGRP). Although we could identify a few CGRP positive axons in the outer laminae of the olfactory bulb, the density of these trigeminal fibers was far too low to account for the AQP1 IR observed in this

region (data not shown). The pattern and density of CGRP IR that we observed were in good agreement with those reported by Shaefer et al. (2002). Therefore, we conclude that the AQP1 expression found in the olfactory bulb does not derive from trigeminal sensory afferent fibers.

Discussion

In the present report we describe the robust expression of a member of the aquaporin family of water channels in the mammalian olfactory system. Using an extensive battery of neuroanatomical tests, we were able to rule out ORNs, OEGs, astrocytes, PG cells, and trigeminal ganglion fibers as the origin of AQP1 IR. Our effort to identify the cell type that expresses AQP1 covered all but one cell type in the olfactory bulb, namely synantocytes. As discussed below, we do not believe synantocytes to be the source of AQP1 in the olfactory bulb. Because our survey is exhaustive, accounting for all known cell and fiber types in the olfactory bulb, we propose that AQP1 may be a marker of a unique, previously unrecognized fiber tract at the interface of the olfactory nerve layer and the glomerular layer of the mouse olfactory bulb.

The remaining cell type that contributes to the neuropil of the olfactory nerve or glomerular layers of the olfactory bulb is the synantocyte, a fourth type of CNS glia (distinguishable from astrocytes, oligodendrocytes, and microglia). Syntanocytes are unique in that they express the chondroitin sulfate proteoglycan NG2 (Horner et al., 2002; Butt et al., 2002; Berry et al., 2002). They are present in the glomerular, external plexiform, and granule cell layers of the olfactory bulb (Treloar et al., 2005). Because neither their distribution nor their stellate shape fits the pattern of AQP1

immunoreactivity, we do not believe that the syntanocyte is the origin of the dense AQP1 IR in the bulb.

It is significant that we never observed cell bodies immunoreactive for AQP1. This likely signifies that either AQP1 protein is transported rapidly to cell processes rather than accumulating in the soma, or that the cells that synthesize AQP1 are located outside of the olfactory bulb and epithelium. Unfortunately our attempts to identify AQP1 mRNA in the olfactory bulb were unsuccessful. In situ hybridization in the olfactory bulb showed non-specific labeling of every cell body (unpublished results), even though we used a probe that provided specific labeling in the dorsal root ganglia and spinal cord (Shields et al., 2006). Thus, although the glomerular layer of the olfactory bulb appears to be one terminus of the fiber tract labeled by AQP1 we cannot yet determine the other terminus, nor the directionality of information flow.

AQP1 has a remarkably limited expression in the mammalian nervous system. Apart from the present report of its presence in fibers of the olfactory bulb, AQP1 has only been described in primary afferent nociceptors (Shields et al., 2006) and a subset of amacrine cells in the retina (Kim et al., 2002). It is of interest that each of these areas is involved in the transmission of sensory information; however, to date we have not uncovered the functional significance of neuronal AQP1 expression. In fact, despite a very comprehensive functional analysis of mice with a deletion of the gene that encodes AQP1, we could not find a behavioral or electrophysiological deficit.

In conclusion, we describe here what appears to be a previously unrecognized and uncharacterized fiber tract in the mammalian olfactory bulb whose sole known marker is AQP1. Future studies should focus on what type

of information is transmitted via these fibers and on the contribution of AQP1 to their function.

References

Agre P, King LS, Yasui M, Guggino WB, Ottersen OP, Fujiyoshi Y, Engel A, Nielsen S (2002) Aquaporin water channels--from atomic structure to clinical medicine. J Physiol 542:3-16.

Anderson SA, Qiu M, Bulfone A, Eisenstat DD, Meneses J, Pedersen R, Rubenstein JL (1997) Mutations of the homeobox genes Dlx-1 and Dlx-2 disrupt the striatal subventricular zone and differentiation of late born striatal neurons. Neuron 19:27-37.

Astic L, Pellier-Monnin V, Godinot F (1998) Spatio-temporal patterns of ensheathing cell differentiation in the rat olfactory system during development. Neuroscience 84:295-307.

Au WW, Treloar HB, Greer CA (2002) Sublaminar organization of the mouse olfactory bulb nerve layer. J Comp Neurol 446:68-80.

Bailey MS, Shipley MT (1993) Astrocyte subtypes in the rat olfactory bulb: morphological heterogeneity and differential laminar distribution. J Comp Neurol 328:501-526.

Berry M, Hubbard P, Butt AM (2002) Cytology and lineage of NG2-positive glia. J Neurocytol 31:457-467.

Buck L, Axel R (1991) A novel multigene family may encode odorant receptors: a molecular basis for odor recognition. Cell 65:175-187.

Bulfone A, Wang F, Hevner R, Anderson S, Cutforth T, Chen S, Meneses J, Pedersen R, Axel R, Rubenstein JL (1998) An olfactory sensory map develops in the absence of normal projection neurons or GABAergic interneurons. Neuron 21:1273-1282.

Butt AM, Kiff J, Hubbard P, Berry M (2002) Synantocytes: new functions for novel NG2 expressing glia. J Neurocytol 31:551-565.

Castle NA (2005) Aquaporins as targets for drug discovery. Drug Discov Today 10:485-493.

Chao TI, Kasa P, Wolff JR (1997) Distribution of astroglia in glomeruli of the rat main olfactory bulb: exclusion from the sensory subcompartment of neuropil. J Comp Neurol 388:191-210.

Halasz N, Ljungdahl A, Hokfelt T, Johansson O, Goldstein M, Park D, Biberfeld P (1977) Transmitter histochemistry of the rat olfactory bulb. I. Immunohistochemical localization of monoamine synthesizing enzymes. Support for intrabulbar, periglomerular dopamine neurons. Brain Res 126:455-474.

Horner PJ, Thallmair M, Gage FH (2002) Defining the NG2-expressing cell of the adult CNS. J Neurocytol 31:469-480.

Huber LJ, Chao MV (1995) Mesenchymal and neuronal cell expression of the p75 neurotrophin receptor gene occur by different mechanisms. Dev Biol 167:227-238.

Kim IB, Lee EJ, Oh SJ, Park CB, Pow DV, Chun MH (2002) Light and electron microscopic analysis of aquaporin 1-like-immunoreactive amacrine cells in the rat retina. J Comp Neurol 452:178-191.

Kosaka K, Toida K, Aika Y, Kosaka T (1998) How simple is the organization of the olfactory glomerulus?: the heterogeneity of so-called periglomerular cells. Neurosci Res 30:101-110.

Long JE, Garel S, Depew MJ, Tobet S, Rubenstein JL (2003) DLX5 regulates development of peripheral and central components of the olfactory system. J Neurosci 23:568-578.

Ma T, Yang B, Gillespie A, Carlson EJ, Epstein CJ, Verkman AS (1998) Severely impaired urinary concentrating ability in transgenic mice lacking aquaporin-1 water channels. J Biol Chem 273:4296-4299.

Margolis FL, Tarnoff JF (1973) Site of biosynthesis of the mouse brain olfactory bulb protein. J Biol Chem 248:451-455.

Matus A, Mughal S (1975) Immunohistochemical localisation of S-100 protein in brain. Nature 258:746-748.

Monti-Graziadei GA, Margolis FL, Harding JW, Graziadei PP (1977) Immunocytochemistry of the olfactory marker protein. J Histochem Cytochem 25:1311-1316.

Mullen RJ, Buck CR, Smith AM (1992) NeuN, a neuronal specific nuclear protein in vertebrates. Development 116:201-211.

Nielsen S, Smith BL, Christensen EI, Agre P (1993) Distribution of the aquaporin CHIP in secretory and resorptive epithelia and capillary endothelia. Proc Natl Acad Sci U S A 90:7275-7279.

Pinching AJ, Powell TP (1971) The neuron types of the glomerular layer of the olfactory bulb. J Cell Sci 9:305-345.

Rubin BD, Katz LC (1999) Optical imaging of odorant representations in the mammalian olfactory bulb. Neuron 23:499-511.

Schaefer ML, Bottger B, Silver WL, Finger TE (2002) Trigeminal collaterals in the nasal epithelium and olfactory bulb: a potential route for direct modulation of olfactory information by trigeminal stimuli. J Comp Neurol 444:221-226.

Shields SD, Mazario J, Skinner K, Basbaum AI (2006) Anatomical and functional analysis of aquaporin 1, a water channel in primary afferent neurons. *Manuscript in preparation.*

Treloar HB, Morton M, Greer CA (2005) NG2-expressing glia in the mouse olfactory bulb. Soc Neurosci Abstr 31:973.910.

Zeitz KP, Guy N, Malmberg AB, Dirajlal S, Martin WJ, Sun L, Bonhaus DW, Stucky CL, Julius D, Basbaum AI (2002) The 5-HT3 subtype of serotonin receptor contributes to nociceptive processing via a novel subset of myelinated and unmyelinated nociceptors. J Neurosci 22:1010-1019.

Zuo Y, Lubischer JL, Kang H, Tian L, Mikesh M, Marks A, Scofield VL, Maika S, Newman C, Krieg P, Thompson WJ (2004) Fluorescent proteins expressed in mouse transgenic lines mark subsets of glia, neurons, macrophages, and dendritic cells for vital examination. J Neurosci 24:10999-11009.

Figure 1. AQP1 immunoreactivity in mouse olfactory bulb.

(A) Sagittal section through the brain reveals AQP1 IR in the trigeminal nucleus caudalis, choroid plexus, and olfactory bulb (arrows). (B) Coronal section through olfactory bulb shows that AQP1 IR is present in the form of a dense meshwork of fine fibers that surround the entire bulb at its superficial surface. (C) Higher magnification of the boxed region in (B) highlights some of the numerous fibers stained for AQP1 in the glomerular layer. (D) These fibers sometimes seem to wrap around individual glomeruli, as shown here. Scale bar in (D) = 10 μm.

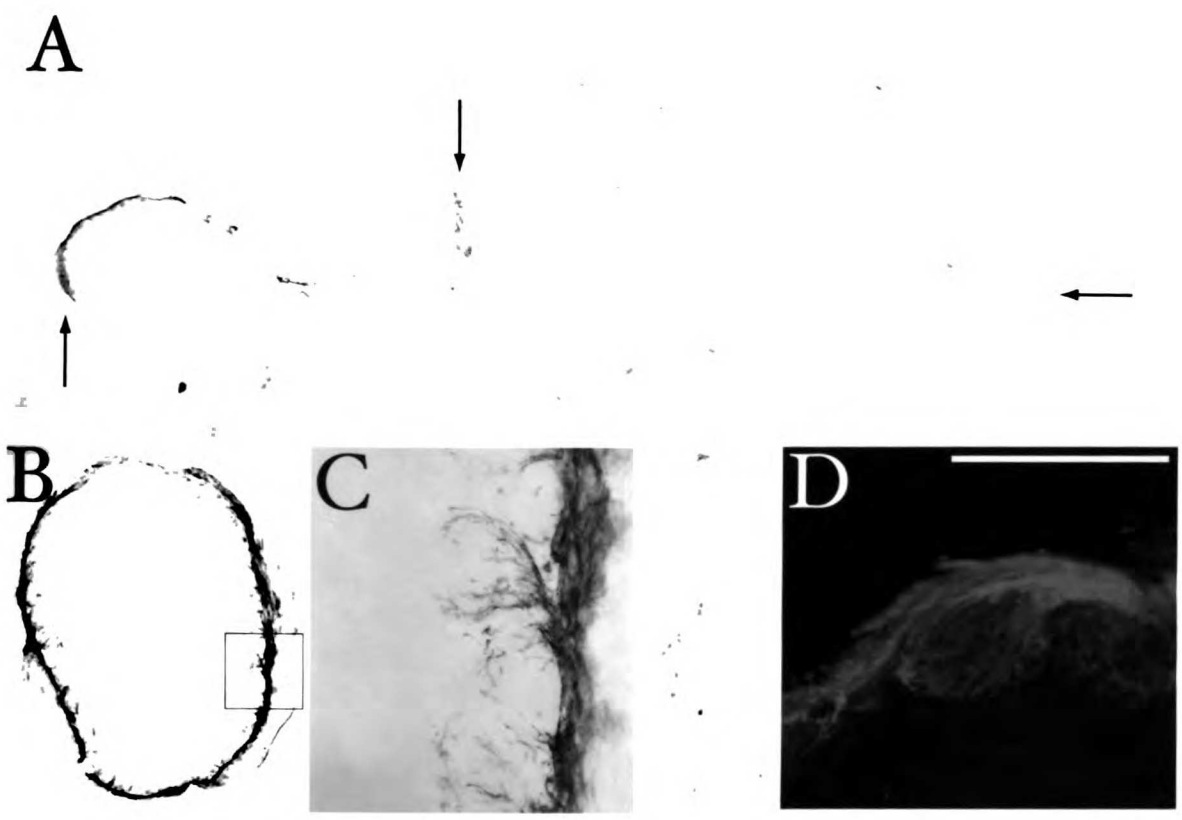
A
B
C
D

Figure 2. AQP1 IR in the olfactory bulb does not derive from ORNs or OEGs.

(A-C) AQP1 and OMP both label a dense band of fibers in the olfactory nerve layer. While OMP fibers (C) clearly innervate glomeruli, AQP1 positive fibers (A) course between glomeruli in a pattern distinct from OMP. (D) The MOE lacks immunoreactivity for AQP1. (E) The MOE does not contain mRNA for AQP1. (F-G) Dissociated OEGs in culture lack AQP1 IR (red, F) while retaining IR for $p75^{NTR}$ (G) Section in (F) is counterstained with DAPI (blue) to show the locations of cell bodies. (H-K) AQP1 staining in Dlx5 mutant mice (J, K) is identical to that seen in littermate controls (H, I).

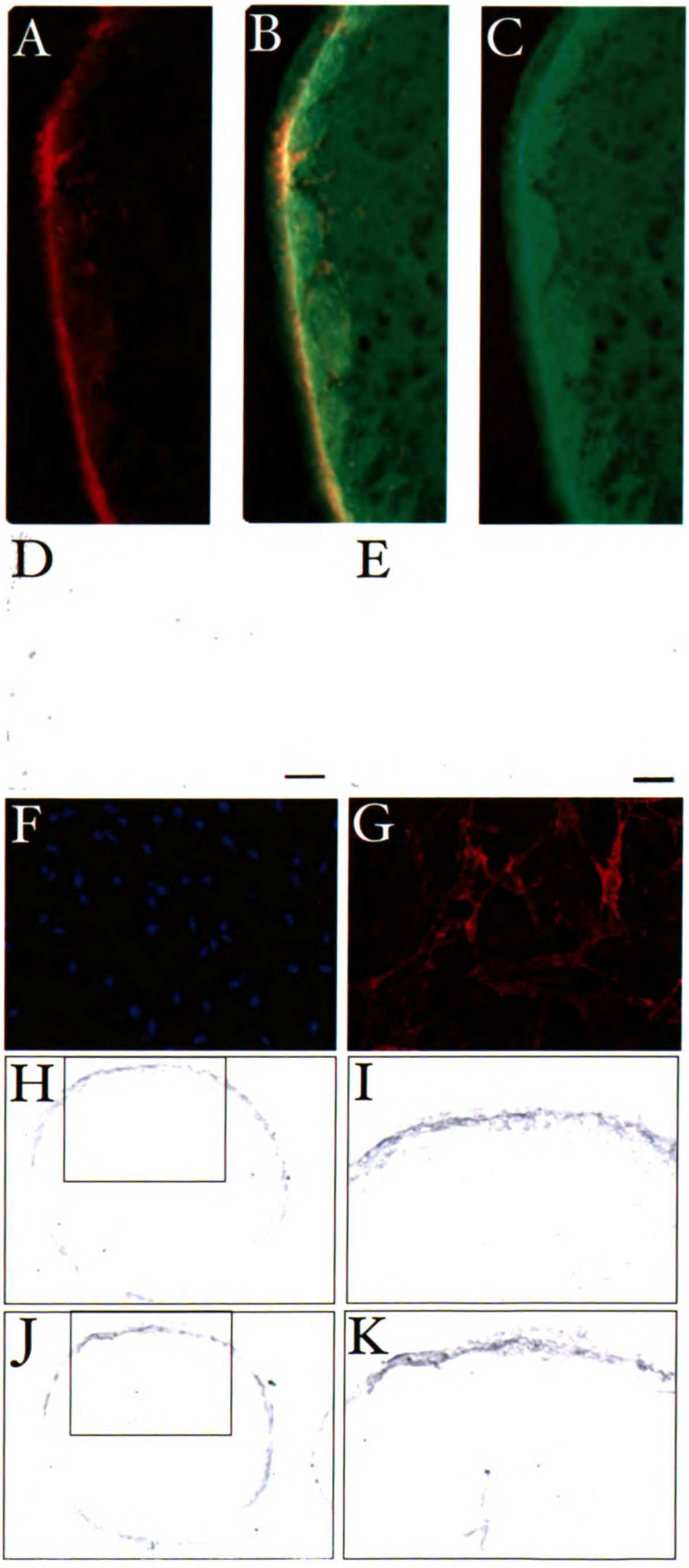
A
B
C
D
E
F
G
H
I
J
K

Figure 3. AQP1 IR in the olfactory bulb does not derive from astrocytes. Sections of the olfactory bulb stained for AQP1 (A) and GFAP (B) reveal distinct patterns of labeling. Scale bar = 20 μm.

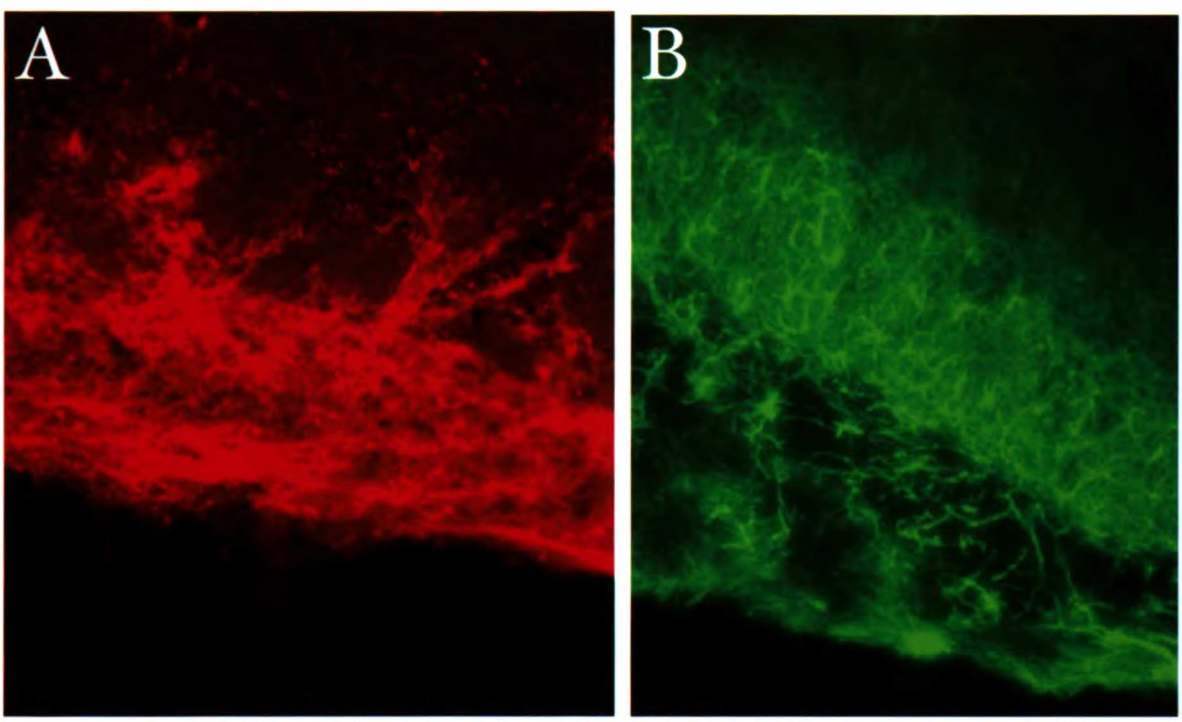
A
B

Figure 4. AQP1 IR in the olfactory bulb does not derive from periglomerular cells. (A-F) AQP1 does not colabel with NeuN (A-C) or TH (D-F), two markers of PG cells. (G-J) AQP1 staining in Dlx1/Dlx2 mutant mice (I, J) is identical to that seen in littermate controls (G, H).

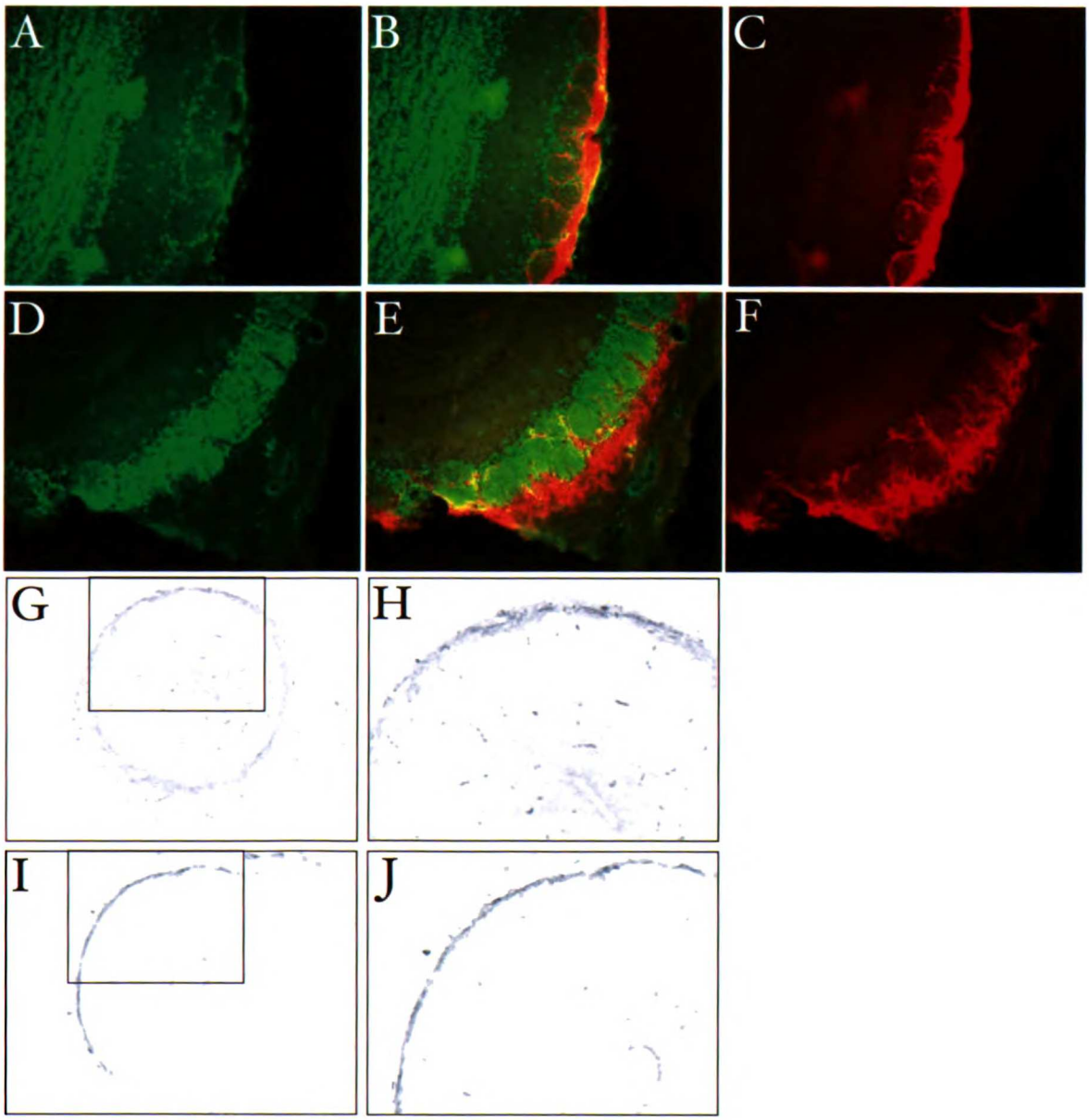
A
B
C
D
E
F
G
H
I
J